Horizon 2020
Programme

GENIORS

Research and Innovation Action (RIA)

This project has received funding from the European Union's Horizon 2020 research and innovation programme under grant agreement No 755171.

Start date : 2017-06-01 Duration : 48 Months
http://geniors.eu/

GENIORS

Product quality, characterization & testing

Authors : Dr. Robin TAYLOR (NNL), H Colledge (NNL), L Walton (NNL), M Sarsfield (NNL), R Taylor (NNL)

GENIORS - Contract Number: 755171

Project officer: Roger Garbil

Document title	Product quality, characterization & testing
Author(s)	Dr. Robin TAYLOR, H Colledge (NNL), L Walton (NNL), M Sarsfield (NNL), R Taylor (NNL)
Number of pages	38
Document type	Deliverable
Work Package	WP7
Document number	D7.4
Issued by	NNL
Date of completion	2021-05-28 16:29:00
Dissemination level	Public

Summary

This report describes experimental trials in which a series of solutions simulating the product from the EURO-GANEX separation process were converted to mixed oxides via the oxalate co-precipitation route. Mixed actinide nitrate solutions containing Pu, Np and lanthanides (Nd and Sm representing the minor actinides Am and Cm) at process-relevant concentrations and ratios were electrochemically conditioned, oxalate co-precipitated and decomposed to mixed oxides before characterisation using a range of standard powder characterisation techniques to assess the quality of the products. Tests were performed with (a) transuranic (and the lanthanide analogues) metals only, (b) TRU and process-relevant ligands (PTD, acetic acid) and (c) TRU and uranium(IV) to produce a (U,TRU) oxide. This study thus provides a good basis for defining a conceptual finishing process for the EURO-GANEX process that can meet product quality specifications based on the oxalate co-precipitation and co-conversion route.

Approval

Date	By
2021-05-31 14:15:06	Dr. Gilles LETURCQ (CEA)
2021-06-08 14:06:51	Dr. Jean-Marc ADNET (CEA)
2021-06-14 11:12:40	Mr. Stéphane BOURG (CEA)

CONTENT

This project has received funding from the EURATOM research and training programme 2014-2018 under grant agreement No 755171. The content of this deliverable reflects only the author's view. The European Commission is not responsible for any use that may be made of the information it contains.

This project has received funding from the EURATOM research and training programme 2014-2018 under grant agreement No 755171. The content of this deliverable reflects only the author's view. The European Commission is not responsible for any use that may be made of the information it contains.

LIST OF FIGURES

This project has received funding from the EURATOM research and training programme 2014-2018 under grant agreement No 755171. The content of this deliverable reflects only the author's view. The European Commission is not responsible for any use that may be made of the information it contains.

LIST OF TABLES

This project has received funding from the EURATOM research and training programme 2014-2018 under grant agreement No 755171. The content of this deliverable reflects only the author's view. The European Commission is not responsible for any use that may be made of the information it contains.

INTRODUCTION

The European Horizon 2020 GENIORS project aims to develop innovative techniques for the recycling of spent nuclear fuel and future multiple recycling strategies to be implemented in a closed nuclear fuel cycle. One of the proposed options being considered is the implementation of fourth generation (GEN IV) nuclear reactors. Here, there is the potential to improve the efficiency of the nuclear fuel cycle by multiple recycling of spent nuclear fuel.

Industrial scale reprocessing is currently dominated by the PUREX process, whereby plutonium and uranium products are separated from spent nuclear fuel as separate streams that are then blended to produce a mixed oxide for use in a reactor. Although this process is effective and well established in terms of industrial experience and technical maturity, the time-consuming blending and milling stage, dusty operations, and inhomogeneity of MOX pellets at higher plutonium concentrations make it undesirable for future advanced recycle technologies. In addition, the perceived proliferation risk associated with producing a separated plutonium stream during reprocessing operations has enhanced the desire to produce co-converted mixed oxides. Advanced reprocessing and recycling technologies provide greater economic benefits, they also generate less wastes for geological disposal and offer greater proliferation resistance than the current PUREX process we use today. It has therefore become an international objective to develop a new hydrometallurgical based process.

One of the more developed advanced processes being considered is the Grouped ActiNide Extraction (GANEX) process, which was initially developed by the Commissariat a l 'energie atomique et aux energies alternatives (CEA) for the hydrometallurgical reprocessing of Gen(IV) spent nuclear fuels. Here, the homogenous recycling of actinides was investigated using two extraction cycles where uranium (VI) is selectively extracted from the dissolution of spent fuel followed by a second extraction cycle where the grouped separation of the transuranic elements (np, Pu, Am, Cm) is achieved prior to co-conversion (Miguirditchian, et al., 2008).

As part of a series European Atomic Energy Community (EURATOM) projects (ACSEPT, SACSESS and GENIORS), funded under European Union Framework Programmes 7 and Horizon 2020, NNL, in collaboration with other partners, has carried out a substantial amount of work researching the GANEX process for the recycle of fast reactor or other advanced fuels. This work has produced the efficient EURO-GANEX process, shown in Figure 1 (taken from (Taylor, et al., 2016).

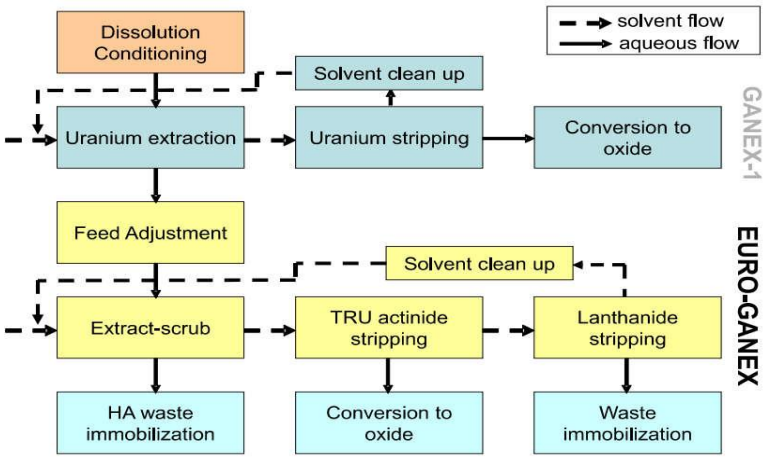

Figure 1: Schematic of the EURO-GANEX flowsheet.

This project has received funding from the EURATOM research and training programme 2014-2018 under grant agreement No 755171. The content of this deliverable reflects only the author's view. The European Commission is not responsible for any use that may be made of the information it contains.

The EURO-GANEX process consists of two stages: the first stage is removing the bulk uranium. This selective uranium extraction is carried using the monoamide solvent N, N-di-(ethyl-2-hexyl) isobutyramide (DEHiBA), which was demonstrated with spent nuclear fuel (Miguirditchian, et al., 2008). Therefore, whilst the first stage of the GANEX process is relatively developed, the second stage of the process is not as straightforward, and this is because it requires the extraction of transuranic actinides (Np-Cm) in oxidation states (III)-(VI).

CEA proposed the use of a mixture of N, N'-dimethyl-N, N'-dioctylhexylethoxy-malonamide (DMDOHEMA) and di(2-ethylhexyl)phosphoric acid (HDEHP) extractants. NNL investigated the potential use of TODGA (N, N, N', N'-tetraoctyldiglycolamide), shown in Figure 2, for the second extraction stage of the GANEX.

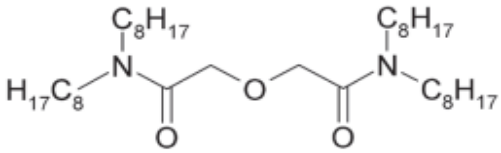

Figure 2: Molecular structure of TODGA

There were however a couple of issues with this extractant. The first issue was that it had rather a low loading capacity for metal ions (Ansari, et al., 2005), (Zhu, Sasaki, Suzuki, & Kimura, 2004), (Modolo, Asp, Schrienemachers, & Vijgen, 2012). Also, it was found to form precipitates with concentrations of Pu(IV) ions above a few grams per litre (Brown, et al., 2012). It was found that in kerosene diluents, TODGA was prone to 3rd phase formation. Following on from previous investigative work on TODGA/TBP solvents systems (Brown, et al., 2010), a range of solvent systems based on diglycolamides with DMDOHEMA, HDEHP, DHOA (N, N-dihexyloctanamide) and TBP were investigated for Pu(IV) loading. The addition of these phase modifiers or co-extractants led to some improvements in Pu loading. From this work the chosen solvent system was 0.2 mol/L TODGA and 0.5 mol/L DMDOHEMA in Exxsol D80 ("odourless kerosene") which showed a good capacity for Pu loading across the nitric acid range used in the process (Figure 3 taken from (Bell, et al., 2012)).

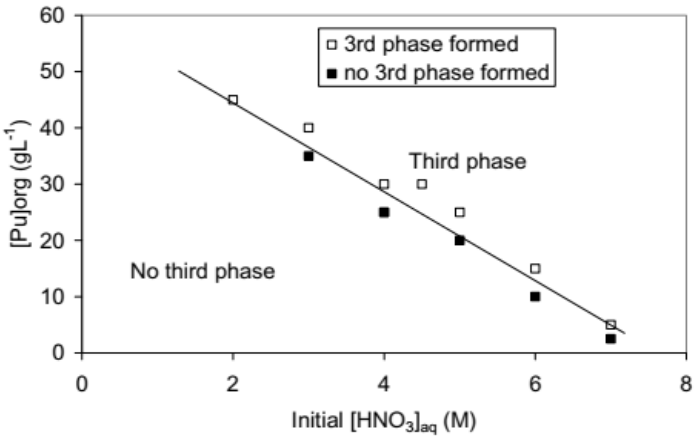

Figure 3: Third phase boundary from Pu(IV) extraction from 2-7 mol L^{-1} HNO_3 in the GANEX solvent (Bell, et al., 2012).

This project has received funding from the EURATOM research and training programme 2014-2018 under grant agreement No 755171. The content of this deliverable reflects only the author's view. The European Commission is not responsible for any use that may be made of the information it contains.

It was found that the Pu loading was significantly increased when combined with the malonamide ligand DMDOHEMA in a kerosene diluent and the forming of precipitation was avoided.

Fission product control is also a key requirement ensuring effective extraction from fission products. Distribution data for key fission products were determined (Carrott, et al., 2015), which showed that most fission products are routed to the aqueous raffinate. Some fission products were co-extracted with the Pu and minor actinides (MA), including iron, strontium, zirconium, palladium, molybdenum, technetium, and ruthenium. Control of iron and strontium was achieved by use of a low acid scrub after the extract section to remove them from the solvent. A complexant 1,2-cyclohexanediaminetetraacetic (CDTA), shown in Figure 4, was added to the active feed as a hold back reagent to suppress the extraction of zirconium and palladium (Wilden, 2015) (Modolo, Wilden, Kaufholz, Bosbach, & Geist, 2014). However, technetium, molybdenum and ruthenium remain problematic and further work is required.

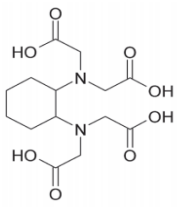

Figure 4: Molecular structure of CDTA.

Selective stripping was also investigated, due to the lanthanides being well extracted by this solvent system. A selective strip is therefore required to achieve separation of lanthanides from the actinides. This was achieved by use of acetohydroxamic acid (AHA) (Figure 5) and a sulphonated bistriazinylpyridine (SO_3-Ph-BTP) ligand (Figure 5) in the development of the EURO-GANEX process (Carrott, et al., 2014). AHA forms strong aqueous soluble complexes with Pu(IV) and also reduces extractable Np(VI) to non-extractable Np(V). The sulphonated BTP ligand selectively strips Am and Cm from the solvent phase and achieves separation from the lanthanides by leaving them in the solvent.

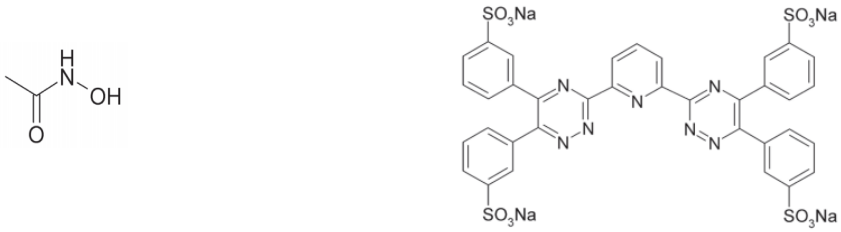

Figure 5: Molecular structure of left) AHA and right) sulphonated BTP.

One of the strategies which is under consideration is for the substitution of SO_3-Ph-BTP with the water soluble complexant 2,6-bis[1-(propan-1-ol)-1,2,3-triazol-4-yl)]pyridine (PyTri-Diol, or PTD), shown in Figure 6. PTD was found to have high actinide selectivity and radiochemical stability and could therefore be suitable for application as a stripping reagent in the EURO-GANEX process (Macerata, et al., 2016), (Wagner, et al., 2017), (Mossini, et al., 2019). Further, PTD is a 'CHON' reagent and therefore decomposes to gaseous products in contrast to the challenging wastes produced using SO_3-Ph-BTP.

This project has received funding from the EURATOM research and training programme 2014-2018 under grant agreement No 755171. The content of this deliverable reflects only the author's view. The European Commission is not responsible for any use that may be made of the information it contains.

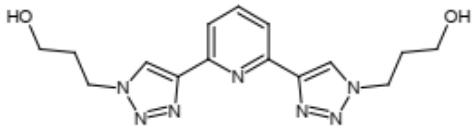

Figure 6: Molecular structure of the aqueous phase complexant PyTriDiol, PTD.

From the investigative work the EURO-GANEX flowsheet as described in the SACSESS Roadmap for actinide separation processes, also shown in Figure 7, was produced (Joly & Boo, 2015). The flowsheet has been demonstrated by Pu active tests in alpha active gloveboxes and a hot test on spent nuclear fuel in hot cells (Malmbeck, et al., 2014) (Malmbeck, et al., 2019). However, the complexants that are used during chemical separations are then carried over into the finishing process.

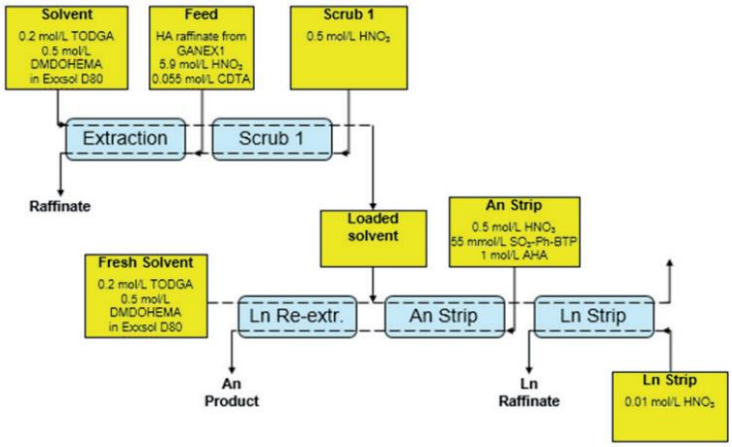

Figure 7: EURO-GANEX chemical separation flowsheet schematic (Joly & Boo, 2015).

Product finishing is the conversion of aqueous metal nitrates into a solid oxide that can either be re-used as fuel or stored prior to disposal and a key challenge is at the interface between solvent extraction and product finishing processes. Plutonium finishing is typically based on an oxalate precipitation process using oxalic acid whereby the plutonium nitrate is converted to a stable oxalate followed by decomposition of the oxalate to the oxide (Arab-Chapelet, Grandjean, Nowogrocki, & Abraham, 2007). Modified versions of the oxalate precipitation route are being investigated for processing the transuranic (TRU) stream Pu, Np, Am and Cm in advanced fuel cycles. Thus, there is a risk that the complexants (or their degradation products) used to strip the TRUs from the solvent phase in the separation stage may perturb the oxalate co-precipitation step through competing complexation. Additionally, the oxalate mother liquor (OML) after filtration needs to be recycled into the separation process. This is to minimise actinide losses to waste streams and to reduce the amount of nitric acid usage in the plant (and hence volumes of aqueous effluents). Residual complexing ligands need to be removed or destroyed prior to recycling nitric acid back into the process. Therefore, strategies are needed to couple the separation and finishing processes, accounting for these issues.

With these potential issues in mind, and as part of the GEN(IV) Integrated Oxide fuel Recycling Strategies (GENIORS) programme, the National Nuclear Laboratory (NNL) have been tasked with the finishing of a GANEX TRU product, looking at the finishing process, product quality and characterisation of the final GANEX product. Experimental work was initiated to consider three GANEX feed experiments containing uranium, plutonium, neptunium and minor actinides (Nd (III) and Sm (III) were used as surrogates for Am(III) and Cm(III)). Three main objectives were set:

This project has received funding from the EURATOM research and training programme 2014-2018 under grant agreement No 755171. The content of this deliverable reflects only the author's view. The European Commission is not responsible for any use that may be made of the information it contains.

1) Assess the effects of temperature and atmosphere during calcination on the characteristics of the mixed oxide products and its ability to maintain a single homogenous oxide phase during conversion.

2) Assess the addition of the complexing ligand (PTD) and the potential degradation product, acetic acid, to determine their effect on the solubility of the metal nitrates and the quality of the oxide produced.

3) Assess the effect of precipitation and calcination of a TRU product with U(IV).

Processing conditions and atmospheres studied are described in Figure 8.

This report describes the work carried out by NNL to support the GENIORS development of finishing a EURO-GANEX TRU product and its characterisation to determine its suitability for re-use as nuclear fuel.

This report looks at the matrix of experiments and discusses the results obtained for the following:

1.) GANEX feed preparation; including plutonium/neptunium co-conditioning and uranium conditioning.
2.) Oxalate precipitation
3.) Oxalate decomposition and calcination
4.) Characterisation

This project has received funding from the EURATOM research and training programme 2014-2018 under grant agreement No 755171. The content of this deliverable reflects only the author's view. The European Commission is not responsible for any use that may be made of the information it contains.

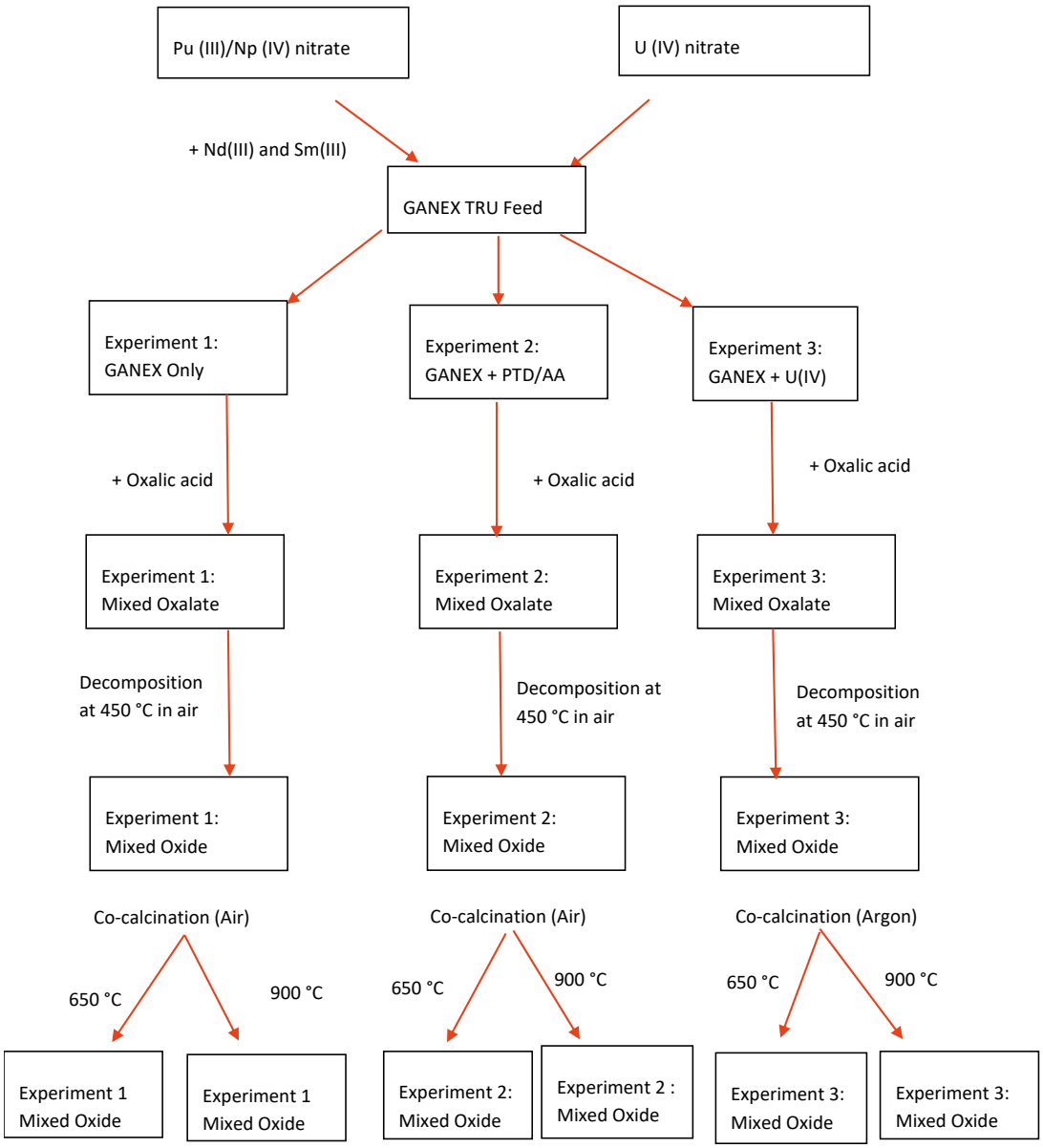

Figure 8: Schematic of planned experiments for the finishing of a EURO-GANEX TRU products

This project has received funding from the EURATOM research and training programme 2014-2018 under grant agreement No 755171. The content of this deliverable reflects only the author's view. The European Commission is not responsible for any use that may be made of the information it contains.

EXPERIMENTAL

GANEX FEED PREPARATION

PLUTONIUM/NEPTUNIUM CONDITIONING

Plutonium (IV) nitrate and neptunium (V) nitrate were electrochemically conditioned to produce a mixed Pu(III)/Np(IV) solution for the preparation of the GANEX TRU feed. Conditioning of neptunium (and uranium) to the tetravalent state prior to oxalate precipitation is necessary due to the relatively high solubility of neptunium(V) oxalate (and uranyl(VI) oxalate) which would lead to unacceptable losses of Np (and U) . Further the adoption of the +4 oxidation state will ensure the co-precipitation of neptunium and uranium to form a homogenous mixed oxalate at the molecular level.

Electrochemical reduction was carried out using a small scale commercial bulk electrolysis cell (ALS SBC cell, supplied by IJ Cambria Scientific) and was used without modification (Figure 9). The glovebox set up can also be seen in Figure 9. The cell comprises of a high surface area reticulated carbon electrode with platinum wire contact and a counter compartment comprising of a glass tube with a fine glass sintered disc containing a platinum wire coil counter electrode. The electrolysis was carried out at constant current and so a reference electrode was not used. The current was supplied using a Solartron 1285 potentiostat with Corr Ware data acquisition. Measurement of the progression of the electrolysis was carried out by periodic sampling and off-line UV-Vis spectrometry, so a 2nd (sensing) working electrode was not used. UV-Vis measurements were carried out using a standard 1 mm quartz cuvette with a fibre optic cuvette holder housed within a fumehood. All measurements were carried out using a Perkin Elmer Lambda 900 UV-Vis-nIR with halogen lamp.

A plutonium (IV) nitrate stock had a starting concentration of 167 g/L, ~ 7 mol/L nitric acid. A neptunium (V) nitrate stock had a starting concentration of 17.9 g/L, 1.9 mol/L nitric acid. These stocks were used to prepare a 75 g/L Pu(III) – 2 g/L Np(IV) – 0.2 mol/L hydrazine nitrate solution by addition of hydrazine hydrate. The hydrazine was added dropwise as a nitrous acid scavenger to stabilise plutonium (III) during electrolysis and after preparation. This solution was transferred to the electrolysis cell with a small amount of 3 mol/L nitric acid as counter electrolyte. Electrolysis was carried out for *ca.3* hours. Samples were taken periodically for determination of the plutonium oxidation state content; this solution was returned to the electrolysis cell after measurement.

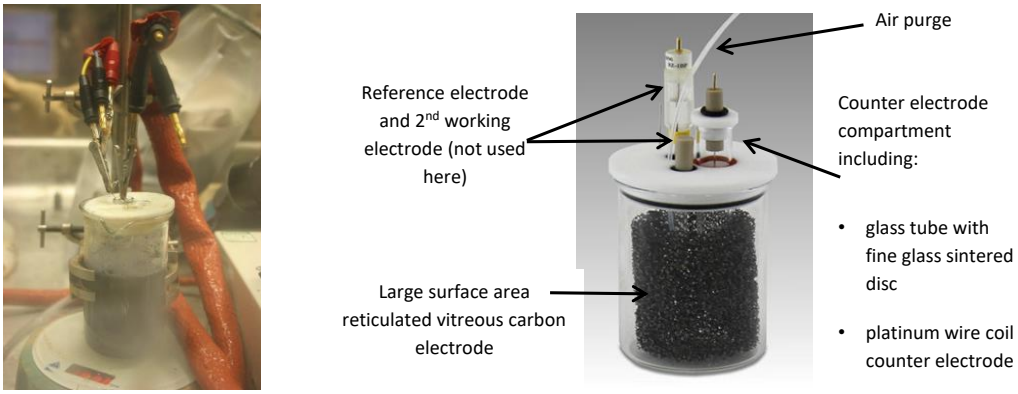

Figure 9: Electrochemical cell: (LHS) diagram of cell (RHS) set up used in glovebox to condition Pu(IV)/Np(V) nitrate.

This project has received funding from the EURATOM research and training programme 2014-2018 under grant agreement No 755171. The content of this deliverable reflects only the author's view. The European Commission is not responsible for any use that may be made of the information it contains.

URANIUM CONDITIONING

The conversion of uranyl (VI) nitrate hexahydrate to U(IV) nitrate was also completed electrochemically using the same set up and process as described above for Pu/Np but in a fumehood. UV-vis measurements were carried out using a Zeiss MCS 501 UV-Vis-nIR spectrometer with halogen lamp.

A uranyl nitrate – water solution was used that had previously been prepared from uranyl nitrate hexahydrate (UNH) dissolved in deionised water. This was used to prepare a 250 g/L – 3.7 mol/L nitric acid – 0.7 mol/L hydrazine nitrate solution by addition of concentrated nitric acid and hydrazine hydrate. The counter electrode compartment was filled with 5 mol/L nitric acid and electrolysis was carried out for *ca.*10 hours over a three-day period.

GANEX FEED

The conditioned U(IV)/Pu(III)/Np(IV) stocks were then used to prepare a 150 mL GANEX TRU feed with the addition of Nd(III) and Sm(III) as surrogates for Am(III) and Cm(III) respectively (Rizkalla & Choppin, 1992). The target concentrations of the various actinides were extrapolated from a previous NNL report modelling the EURO-GANEX flowsheet, as detailed in reference (FRFR2: gPROMS model of GANEX process developed, 2020), with the ratios of each species kept constant but at reduced concentrations compared to the flowsheet values (Table 1). This was due to previous challenges experienced in preparing a high concentration Pu(IV) stock. The final stock was made up to volume using 0.5 mol/L nitric acid.

Table 1: Components to prepare GANEX feed.

	concentration (g/L)	% mol/L	Mass of element (g)	Volume of stock (mL)
U(IV)	0.14	0.16	0.021	0.12
Pu(III)	75.00	86.30	11.250	67.0
Np(IV)	1.95	2.26	0.292	16.3
Nd(III)	3.72	7.09	0.558	-
Sm(III)	2.29	4.19	0.344	-

A second feed was then prepared by dilution of the GANEX feed described above with U(IV) nitrate. This was done to mimic the down blending of fuel to make suitable targets for irradiation in a fast reactor that would enable the transmutation of minor actinides (Table 2). The feed was made up to volume with 0.5 mol/L nitric acid.

Table 2: GANEX:U(IV) feed components.

	% mol/L	Volume of stock (mL)
U(IV)	66.4	25.27
GANEX Feed	33.6	18.70

This project has received funding from the EURATOM research and training programme 2014-2018 under grant agreement No 755171. The content of this deliverable reflects only the author's view. The European Commission is not responsible for any use that may be made of the information it contains.

OXALATE PRECIPITATION

Three experiments were considered during this project:

- oxalate precipitation of a GANEX TRU feed (prepared according to Table 1),
- oxalate precipitation of a GANEX TRU feed in the presence of PTD and acetic acid
- oxalate precipitation of a GANEX TRU feed co-precipitated with 66 mol % U(IV)

The experimental volumes are summarised in Table 3.

Table 3: Experimental volumes used during co-precipitation of the GANEX TRU feed.

Experiment	Volume GANEX TRU Feed (mL)	Mass of PTD (g)	Volume of glacial acetic acid (17.4 mol/L) (mL)	Volume of 0.6 mol/L oxalic acid (mL)	Total volume (mL)
1 (GANEX only)	61.2	0.0	0.0	108.3	169.5
2 (GANEX + PTD/AA)	61.2	3.1	0.5	108.3	170.1
3 (GANEX + U(IV))	30.6	0.0	0.0	108.3	138.9

A simple batch scale set up was used consisting of a stirrer plate and beaker for each of the experiments shown in Figure 10. The required volume of the GANEX nitrate feed plus U(IV) stock solution (if required) plus PTD/acetic acid (if required) were added into the beaker and stirred at 300 rpm at ambient temperature. Oxalic acid (0.6 mol/L) was then added to promote precipitation. This is the direct strike method where oxalic acid is added into the heavy metal feed. Each solution was stirred for a set period of 1 hour (Figure 10). Once equilibrium was reached, the solid precipitate was filtered through a vacuum Buchner funnel with a Duran sintered filter into a Buchner flask. The solid was washed with ~20 mL of 0.5 mol/L HNO_3 and ~20 mL of de-ionised water and allowed to dry under vacuum for ~30 minutes. The solid oxalate precipitate was then left to dry in a petri dish for a couple of days and then weighed into an aluminium sample container for analysis / prior to decomposition. The collected oxalate mother liquor (OML) was filtered through a 0.45 µm Sartorius 0.45 µm syringe filter and diluted in 0.1 mol/L nitric acid and analysed by ICP-MS and UV-Vis spectroscopy.

Figure 10: Batch scale oxalate co-precipitation set up (beaker contains Experiment 3: GANEX + U(IV))

This project has received funding from the EURATOM research and training programme 2014-2018 under grant agreement No 755171. The content of this deliverable reflects only the author's view. The European Commission is not responsible for any use that may be made of the information it contains.

OXALATE DECOMPOSITION AND CALCINATION

Due to the production of carbon monoxide during the decomposition of oxalate compounds and the potential deflagration risk this poses in the glovebox environment, any oxalates produced must be decomposed on a hotplate up to 500 °C prior to calcination in a tube furnace at higher temperatures (NNL Central Laboratory safety case requirement). For this experimental programme an air atmosphere was used during the decomposition stage to drive off any carbon produced during decomposition. Different atmospheres and temperatures were used for the calcination stages to investigate their combined effect on the final mixed oxide product.

Each mixed oxalate was loaded into an Inconel crucible and decomposed on a hotplate at 450 °C and held at temperature for 3 hours. The green solid converted into a black granular powder indicating the successful decomposition of the oxalate (Figure 11). No further analysis was carried out at this stage to confirm whether any residual oxalate was remaining.

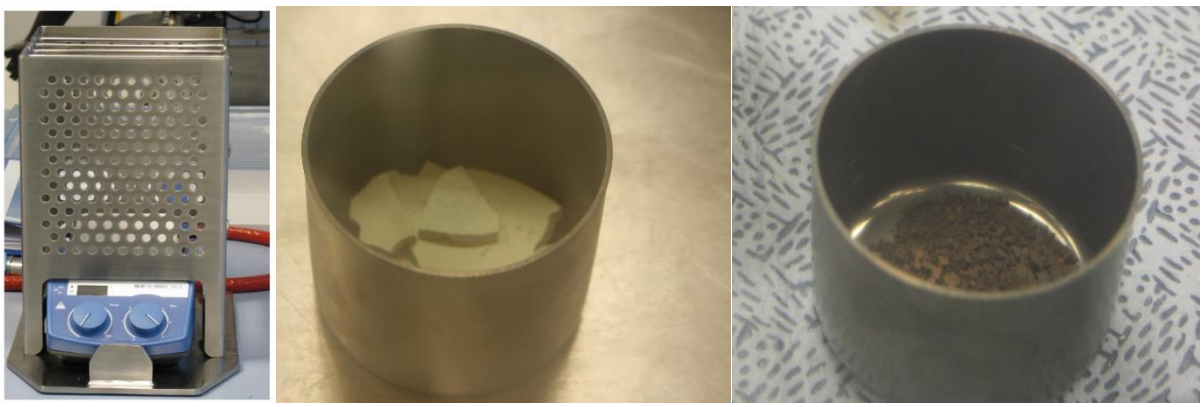

Figure 11: From left to right: Hotplate and associated guard used for decomposition; mixed (U,Pu,Np) oxalate in Inconel crucible prior to decomposition; mixed (U,Pu,Np) oxide in Inconel crucible after decomposition.

Following decomposition, for each oxalate, the material was halved and calcined in an Instron tube furnace at 650°C and 900 °C under an air or argon glovebox atmosphere (Figure 8). A ramp rate of 20 °C/min and a two hour hold at the target temperature was used for each sample.

ANALYSIS TECHNIQUES

The oxalate mother liquor, mixed oxalate solids and the mixed oxides were sent for a variety of different analyses to characterise the products as described below.

INDUCTIVELY COUPLED PLASMA-MASS SPECTROMETRY (ICP-MS)

The oxalate mother liquor (OML) was analysed by ICP-MS to determine the extent of precipitation by determining percentage recovery of the metal ions in the precipitate and any losses to the OML due to actinides ions that remained in solution following the precipitation step.

ICP-MS has been developed to provide an ionisation efficiency of over 90% for most elements which gives the instrument a wide range of detection for all necessary analysis. The standard matrix when running through the ICP-MS is a solution of 2% nitric acid.

This project has received funding from the EURATOM research and training programme 2014-2018 under grant agreement No 755171. The content of this deliverable reflects only the author's view. The European Commission is not responsible for any use that may be made of the information it contains.

X-RAY DIFFRACTION (XRD)

Samples of the mixed oxalates / oxides were analysed by XRD to determine the structure of the different products. NNL's X-ray powder diffractometer is an open bench instrument and therefore alpha containing samples must undergo a rigorous preparation process to encapsulate the material to prevent the spread of loose alpha contamination during analysis. Containment of the mixed (U,Pu,Np) samples during analysis was achieved by encapsulating the powder in epoxy resin to form a puck that is secured into a plexi-glass ring, as shown in Figure 12. The puck was then swabbed and monitored to confirm contamination levels below 5 cps prior to posting out of the glovebox for analysis.

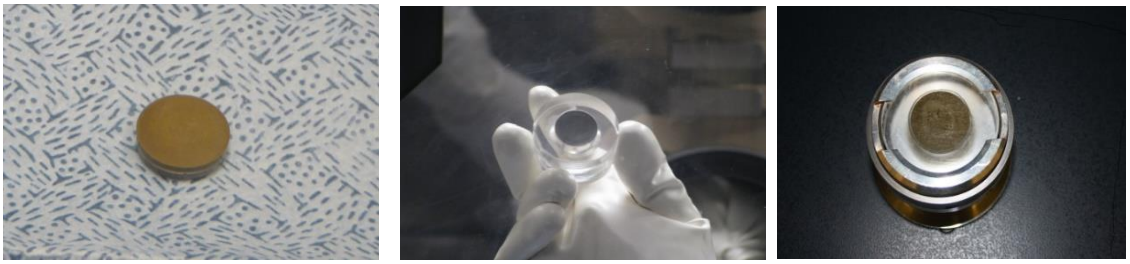

Figure 12: From left to right: PuO_2 powder encapsulated in an epoxy resin; sample puck fixed into a plexi-glass ring; sample puck contained in a magnetic XRD sample holder on the open bench.

X-ray diffraction patterns were recorded using an open bench Bruker D8 Advance diffractometer operating with a Cu $K\alpha$ X-rays. Powder patterns were recorded between 5° and 60° (for oxalate samples) and 25° and 145° (for oxide samples).

Analysis of the diffraction patterns to determine the structure of the TRU oxides was carried out using the Bruker TOPAS 5.0 software. First the zero off-set was determined using a Standard Reference Material (SRM), corundum (Al_2O_3), which requires the diffraction angle of each peak to be measured. This was performed using "single peak fitting" of the diffraction pattern. This means that the diffraction pattern is modelled with the position of each peak fitted independently (i.e. without controlling the peak position using knowledge of the structure). Line shape effects are also included so that asymmetry is considered in the line position. After the peak positions are determined a plot of θ_true-2θ_exp against cos(θ) is drawn. The intercept of this graph is equal to the zero offset of the diffractometer.

Following the determination of the zero-offset, the SRM diffraction pattern was fitted using the Pawley whole pattern fitting refinement to calculate the lattice parameter and optimised instrument parameters. Pawley fitting involves the position of all the peaks in the pattern being calculated from the crystal lattice and symmetry, with the lattice parameters optimised, but the intensity of each peak optimised independently. The refined instrument parameters and zero-offset calculated using SRM were subsequently fixed and used in the whole pattern fitting of the mixed TRU oxide samples using the Pawley fitting method.

FOURIER TRANSFORM INFRARED ANALYSIS (FTIR)

Fourier Transform Infrared Analysis was carried out with IR spectra recorded on an Agilent Cary 630 FTIR Spectrometer with the use of a diamond Attenuated Total Reflectance (ATR) accessory. Measurements were recorded between 650 cm^{-1} and 4000 cm^{-1} in transmission mode with 4 cm^{-1} steps.

This project has received funding from the EURATOM research and training programme 2014-2018 under grant agreement No 755171. The content of this deliverable reflects only the author's view. The European Commission is not responsible for any use that may be made of the information it contains.

For the oxalate samples the data has been normalised to allow comparison of all the peaks. No normalisation was applied to the oxide samples.

SPECIFIC SURFACE AREA (SSA) ANALYSIS

Analysis of specific surface area within the NNL High Alpha Inventory Laboratories used a modified Micromeritics Gemini VII 2390a analyser. Samples of ~1 g were degassed under vacuum at 300 °C for >4 hours prior to analysis. Analysis used nitrogen as the adsorbate gas at 77 K with analysis over a partial pressure range p/p_0 0.05 to 0.3. Specific surface area was obtained from a BET plot of the isotherm values.

SELLAFIELD ANALYTICAL SERVICES – CARBON ANALYSIS

Samples (~0.4 g oxide) were sent to Sellafield Limited Analytical Services (SLAS) to be analysed using an accredited procedure. Here, the samples are exposed to high purity oxygen at 950 °C and the carbon dioxide evolved is determined by absorption and electrolytic titration using a Coulomat analyser.

This project has received funding from the EURATOM research and training programme 2014-2018 under grant agreement No 755171. The content of this deliverable reflects only the author's view. The European Commission is not responsible for any use that may be made of the information it contains.

RESULTS AND DISCUSSION

PLUTONIUM / NEPTUNIUM CONDITIONING

The reduction of Pu(IV)/Np(V) to Pu(III)/Np(IV) was monitored by off-line UV-vis spectroscopy and the overlaying results are shown in the UV-Vis absorbance spectra in Figure 13. This shows the disappearance of the plutonium(IV) absorption band centred at 475 nm (red arrow) and the ingrowth of a doublet absorption bands at 570, 600 nm (blue arrow); a singlet at 665 nm, a broad doublet at 770, 815 nm and a single peak at 900 nm (blue arrow); all characteristic of Pu(III). Further there was no evidence of a sharp peak at 833 nm that would have indicated oxidation to Pu(VI) instead of reduction (Taylor & Kay, 1998). There were no obvious neptunium absorption bands likely due to the much higher concentration of plutonium (III) used in the TRU feed in comparison to neptunium. Plotting the peak absorbances for plutonium(IV) (475 nm) and plutonium(III) (570 and 900 nm) against time showed quantitative conversion and stabilisation to plutonium(III). The conversion was also detected by a distinct colour change from brown/red to blue, characteristic of the reduction of Pu(IV) to Pu(III) respectively. Conditioning was carried out at 0.5 amps and was monitored closely as prolonged exposure to the current resulted in the immediate destruction of the hydrazine stabiliser and reformation of Pu(IV).

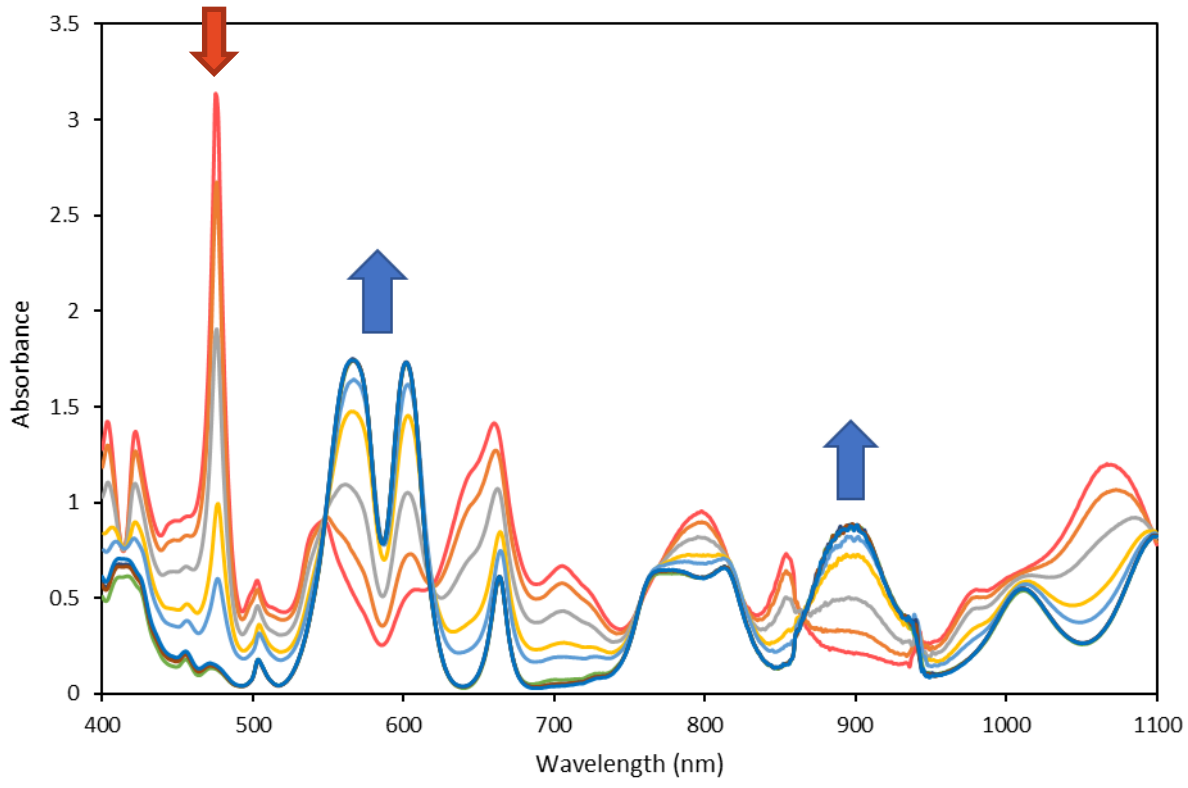

Figure 13: UV-vis absorbance spectra for the electrochemical conditioning of Pu(IV)/Np(V) to Pu(III)/Np(IV).

This project has received funding from the EURATOM research and training programme 2014-2018 under grant agreement No 755171. The content of this deliverable reflects only the author's view. The European Commission is not responsible for any use that may be made of the information it contains.

URANIUM CONDITIONING

During electrolysis of uranium, a visible colour change from an iridescent yellow colour to green was observed characteristic of U(VI) and U(IV) respectively. The conversion was also monitored by UV-vis spectroscopy and the overlaying results are shown in the UV-Vis absorbance spectra, Figure 14. This shows the disappearance of the uranium(VI) absorption band centred at 416 nm (yellow arrow in Figure 14) with lots of fine structure to the multi-banded uranium(IV) absorption spectra with peaks centred at 476 nm, 545 and 646 nm (green arrows in Figure 14). There is a large gap between the start of the conversion and the end due to issues with the UV-vis spectrometer however, plotting the peak absorbances for uranium(VI) (416 nm) and uranium(IV) (476 and 646 nm) against time showed quantitative conversion to uranium (IV). The uranium(VI) content in uranium(IV) solutions cannot be easily determined by UV-Vis absorbance spectrometry due to the overlap of the uranium(IV) and (VI) absorbance bands.

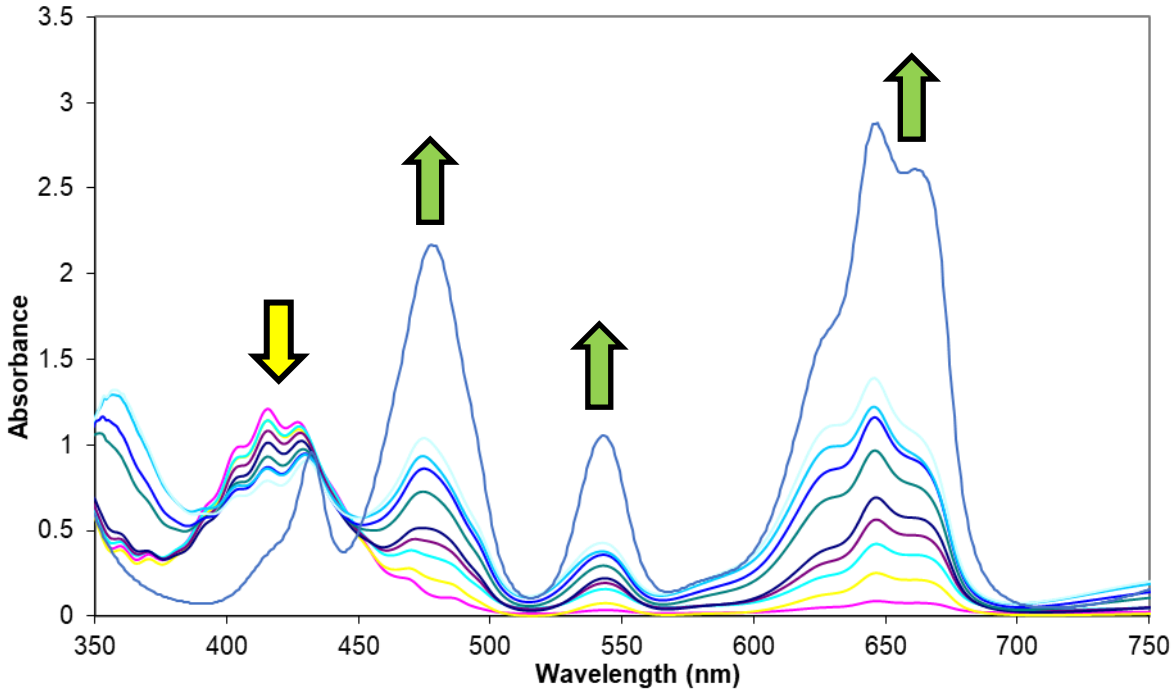

Figure 14: UV-vis absorbance spectra showing the reduction of U(VI) to U(IV) nitrate.

GANEX FEED

The combined GANEX TRU feed including Pu(III)/Np(IV)/U(IV)/Nd(III)/Sm(III) ions had an overall acidity of 1.3 mol/L and a final Pu(III) concentration of 70 g/L. The concentration of Pu(III) was determined using the Pu(VI)/Ce(IV) method as described in reference (Dhamodharan & Pius, 2016). This method relies on the oxidation of Pu(III) to Pu(VI) by addition of ammonium cerium (IV) nitrate and analysis by UV-vis spectroscopy. Comparison of the absorption bands of 830.50 nm and 810.01 nm allowed the calculation of the Pu content of the feed. This method has an inaccuracy of ±5% but allows for reassurance of Pu concentration prior to further processing. The second U(IV)/GANEX TRU feed had a final acidity of 2.0 mol/L.

This project has received funding from the EURATOM research and training programme 2014-2018 under grant agreement No 755171. The content of this deliverable reflects only the author's view. The European Commission is not responsible for any use that may be made of the information it contains.

OXALATE PRECIPITATION

A simple batch scale precipitation process was used for all three experiments with each one completed consecutively on the same working day to minimise any ingrowth of Pu(IV) in the feed. Following the addition of all components into the beaker, a UV-vis spectrum was recorded for each experiment prior to the addition of oxalic acid (Figure 15). A second UV-vis spectrum of the oxalate mother liquor (OML) was recorded after precipitation and the spectra can be seen in Figure 16.

From Figure 15, for experiments 1 and 2, the feed to the precipitator (breaker) remained as predominantly Pu(III) with a small ingrowth of Pu(IV) at 475 nm since preparing the original feed. For experiment 2 there was also a large tail at ~450 nm that was also present in the OML following precipitation, Figure 16. Since this peak was only present in experiment 2 this suggests this was caused by the presence of PTD or acetic acid in the feed, which is supported by the fact that the OML had a distinct yellow colour that is characteristic of PTD. Experiment 3 contained U(IV) as shown by the presence of the absorbance bands at 480 and 650 nm with no evidence of U(VI) formation. The unusual peaks at ~950 nm are due to a lamp change during analysis. Apart from the potential PTD peak in Figure 16 no other components were detected in the OML for each experiment and is as expected.

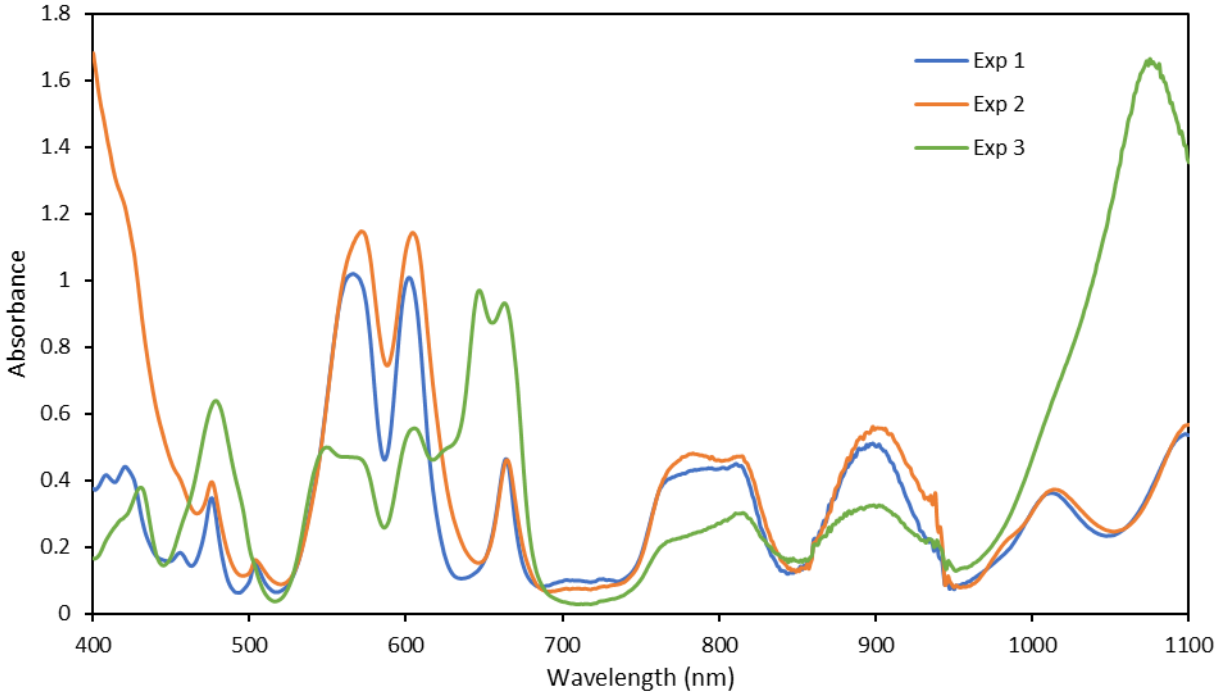

Figure 15: UV-vis absorbance spectra of each experiment prior to the addition of oxalic acid.

This project has received funding from the EURATOM research and training programme 2014-2018 under grant agreement No 755171. The content of this deliverable reflects only the author's view. The European Commission is not responsible for any use that may be made of the information it contains.

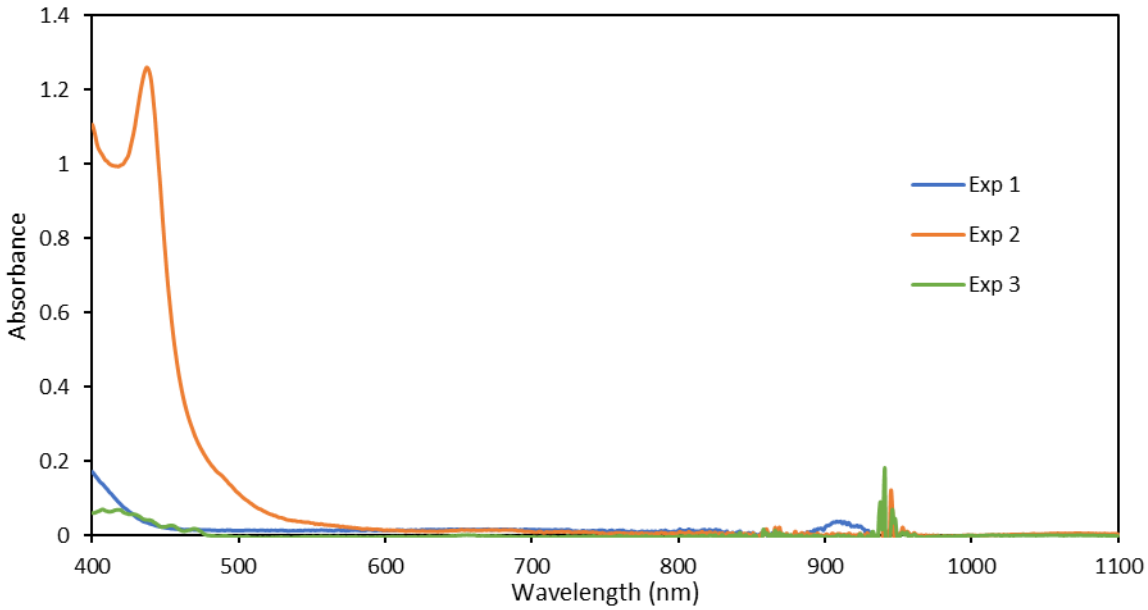

Figure 16: UV-vis absorbance spectra of the oxalate mother liquor (OML) from each experiment following oxalate precipitation.

The precipitate filtered easily with no visible loss of solid to the OML. In addition to UV-vis analysis, Inductively Coupled Plasma-Mass Spectrometry (ICP-MS) was carried out on the OML to calculate the percentage recovery of metal ions in the precipitate and any losses to the OML. The results for Pu, Np and U are presented in Table 4; Sm and Nd were below the limit of detection (LOD) of the spectrometer and are therefore not reported here. The results show excellent recovery of the metal nitrates to the precipitate with minimal losses to the OML. Here, 20% oxalic acid excess was used and likely attributes to the high recovery.

Table 4: ICP-MS results for Pu, Np and U from the oxalate mother liquor.

Experiment	Plutonium			Neptunium			Uranium		
	[Pu] in OML g/L	%loss to OML of Pu	% Recovery	[Np] in OML g/L	%loss to OML of Np	% Recovery	[U] in OML g/L	%loss to OML of U	% Recovery
1	0.53	0.71%	99.29%	0.05	2.61%	97.39%	0.34	<LOD	100%
2	0.43	0.58%	99.42%	0.02	1.05%	98.95%	0.20	<LOD	100%
3	0.34	1.69%	98.31%	0.01	2.10%	97.90%	1.27	1.04%	98.96%

The oxalate solids can be seen directly after filtration in Figure 17. Experiment 1 was a dark green precipitate characteristic of the high plutonium content of the GANEX TRU feed, whereas experiment 2 included the same concentration of Pu with the addition of PTD and acetic acid and had a lighter colour precipitate. Experiment 3 was a light green solid and is characteristic of the higher uranium content (73%). All solids dried in the glovebox atmosphere over a 2 day period before sampling for analysis by FTIR spectroscopy and XRD.

This project has received funding from the EURATOM research and training programme 2014-2018 under grant agreement No 755171. The content of this deliverable reflects only the author's view. The European Commission is not responsible for any use that may be made of the information it contains.

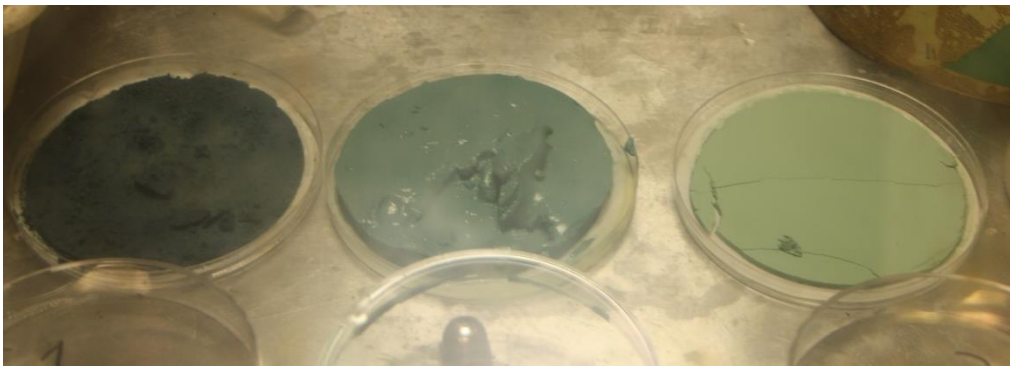

Figure 17: Oxalate solids directly after filtration; from left to right, experiments 1, 2 and 3.

INFRARED SPECTROSCOPY

The dried GANEX TRU oxalates were analysed by FTIR spectroscopy. The infrared spectra, as shown in Figure 18 and Figure 19, are characteristic of oxalate compounds as indicated by the infrared bands located at 480, 795 , 1310, 1350, ~1475 and 1600 cm^{-1} and is in good agreement with literature reports on mixed oxalate compounds (Arab-Chapelet, Grandjean, Nowogrocki, & Abraham, 2008), (Vigier, Grandjean, Arab-Chapelet, & Abraham, 2007). When comparing the absorption bands centred at 1350 and 1310 cm^{-1} for experiment 1 and 2 which were predominantly 90% Pu(III) mixed oxalate this indicates a tetragonal structure whereas experiment 3 which was predominantly 73% U(IV) appears to have a hexagonal structure. This is further confirmed by the shift in the absorption band at ~1450 cm^{-1} and is in agreement with literature data (Arab-Chapelet, Grandjean, Nowogrocki, & Abraham, 2007). The presence of additional absorption bands at 950 and 910 cm^{-1} could be assigned to the N-N stretching vibration resulting from the presence of hydrazinium cations ($N_2H_5^+$) within the mixed oxalate structure. Similar observations have been observed in the literature but at slightly higher wavenumbers reported as 960 and 930 cm^{-1} respectively (Arab-Chapelet, Grandjean, Nowogrocki, & Abraham, 2008), (Govindarajan, Patil, Poojary, & Manohar, 1986). The broad peak present in each spectrum at 3000-3500 cm^{-1} can be associated with water molecules within the structure. Each experiment contained low concentrations of Nd(III) and Sm(III) as part of the original GANEX TRU feed and the presence of a weak peak at 1090 cm^{-1} is likely from the presence of the lanthanides (III) but it is too weak to confirm this. Experiment 2 included the addition of PyTriDiol (PTD) and acetic acid. An absorption band at 1520 cm^{-1} can be assigned to the C-C, C-N, N-N bonds in the pyrazole ring in PTD (Figure 6) (Krishnakumar, Jayamani, & Mathammal, 2011) further absorption bands around 3000cm^{-1} due to the presence of C-H, N-H and O-H bonds are expected for PTD but these are likely masked by the broad water molecule absorption band. An additional peak at 1024 cm^{-1} is only present in experiment 2 and from the literature could be a bridging nitrate group from the presence of PTD. For acetic acid shoulders at 1270 cm^{-1} and 1170 cm^{-1} are characteristic of acetic acid (Jaffe & Rose, 1991) with a potential third shoulder at ~1700 cm^{-1}. Additional bands at 1065 and 1120 cm^{-1} are indicative of a primary and secondary alcohol group, C-O, that could be from either the PTD or acetic acid.

This project has received funding from the EURATOM research and training programme 2014-2018 under grant agreement No 755171. The content of this deliverable reflects only the author's view. The European Commission is not responsible for any use that may be made of the information it contains.

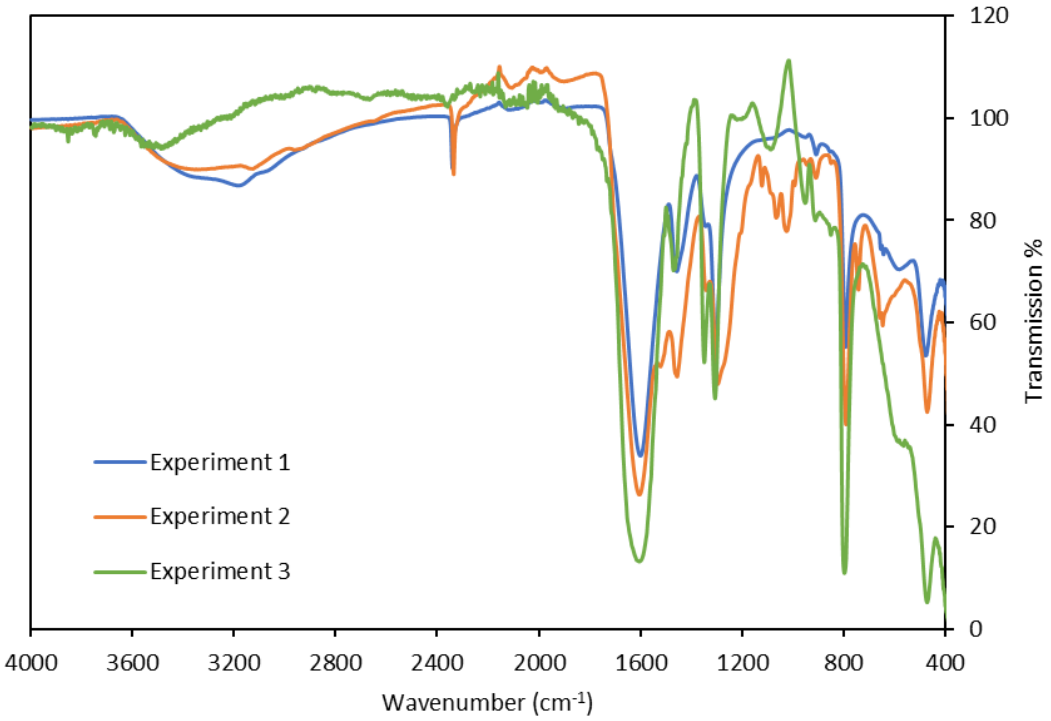

Figure 18: Infrared spectra of each oxalate solid produced from oxalate precipitation of the GANEX feeds.

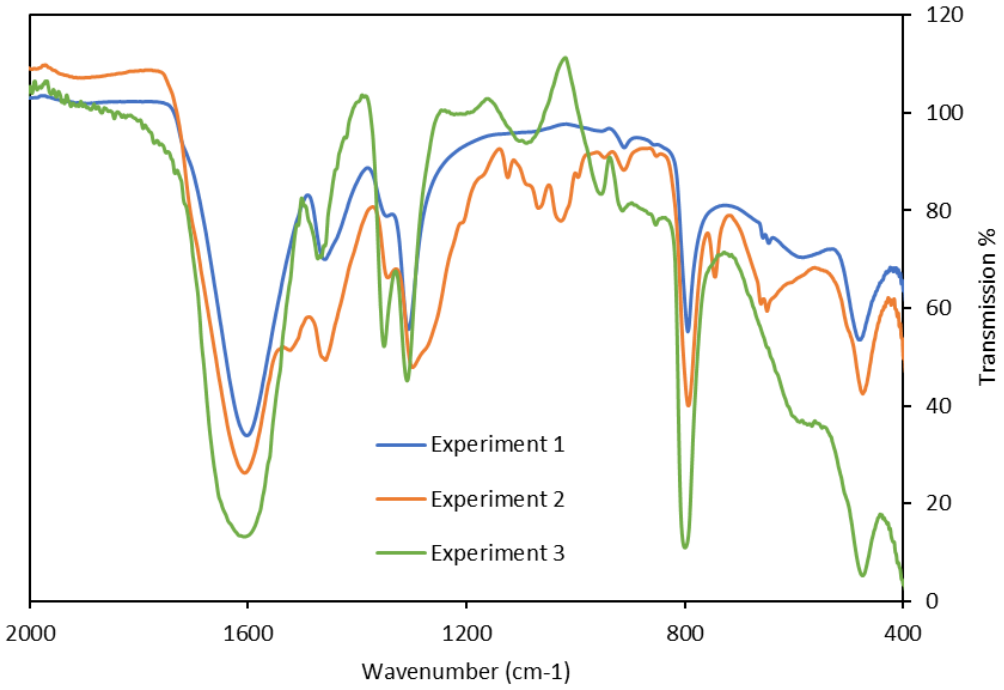

Figure 19:Infrared spectra of each oxalate solid between 400-2000 cm^{-1}

This project has received funding from the EURATOM research and training programme 2014-2018 under grant agreement No 755171. The content of this deliverable reflects only the author's view. The European Commission is not responsible for any use that may be made of the information it contains.

Table 5: Infrared absorption data on GANEX oxalates.

Wavenumber/ cm^{-1}	Observed bands			Tentative assignment
	Exp 1	Exp 2	Exp 3	
3450			br	H_2O
3200	m, v br	m, v br	m, v, br	H_2O - overlap of various water coordination and vibration modes including H-bonded
2640		vvw		
2340	m	m		possibly atmospheric CO_2
1600	s	s	s	overlap of asymmetric ν(C-O) and bending δ(H-O-H)
1520		s		C-C, C-N, N-N from pyrazole ring on PTD
1475	m/w			symmetric ν oxalate C-O, terminal (C-O-M)
1455		s	s	symmetric ν oxalate C-O, terminal (C-O-M)
1350	m	m	m	symmetric ν(C-O), oxalate, bridging
1310	s		s	symmetric ν(C-O), oxalate, bridging/terminal
1300		s		symmetric ν(C-O), oxalate, bridging/terminal
1270		sh		C-N stretch/ bridging nitrate, acetic acid
1205		sh		C-N maybe
1170		sh		acetic acid
1120		w		C-O, secondary alcohol
1090	sh	sh	w, br	Nd/Sm oxalate peak, potentially ν(C-O)
1065		m/w		C-O, primary alcohol
1020		m/w		bridging nitrate
993		w		
950	s	s	s	
910	w	w	w	
795	s	s	s	δO-C-O oxalate and ν M-O
740		m		C-H bending
650	w	w		possibly Nm/Sm oxalate specific peak, probably νM-O
640	w	w		possibly Nm/Sm oxalate specific peak, probably νM-O
590	m		w, br	
480	s	s	s	symmetric δ C-C-O and νM-O
360-370 region	s	s	s	possibly δO-C-O and/or νM-O

Note: s-strong; m-medium; w-weak; vw--very weak; br--broad; v br--very broad; vvw --very weak; sh-shoulder

This project has received funding from the EURATOM research and training programme 2014-2018 under grant agreement No 755171. The content of this deliverable reflects only the author's view. The European Commission is not responsible for any use that may be made of the information it contains.

X-RAY DIFFRACTION

X-Ray diffraction analysis was completed on each of the mixed oxalates and the diffraction patterns are presented in Figure 20. Due to the encapsulation process, a broad hump was present between 10 – 30 2Θ from crystallisation of the epoxy resin within each sample puck; this has been removed using Bruker TOPAS-5 software. For experiments 1 and 2 this was more challenging due to the limited number of strong peaks within the diffraction pattern which also makes assignment rather difficult (Figure 20). The weak diffraction patterns for experiments 1 and 2 suggest that the powder samples have low crystallinity. On consultation with the literature this is a common occurrence in An(IV)-An(III) oxalates and is a consequence of sample preparation and partial radiolysis caused by certain isotopes giving a low signal to background ratio (Arab-Chapelet, Grandjean, Nowogrocki, & Abraham, 2008) (Tamain, Grandjean, Arab-Chapelet, & Abraham, 2010). Experiments 1 and 2 were composed of predominantly An(III) and Ln(III) metal ions comprising of ~97% of the oxalate compound, due to the challenges in refining the pattern it is difficult to draw conclusions on the structure of the mixed oxalates formed. Experiment 3 comprised of a U(IV) – An/Ln(III) oxalate and is in excellent agreement with XRD data reported in the literature for a 70% U(IV)/30% Pu(III) mixed oxalate structure and suggests the formation of a hexagonal structure with the generic formula $M_{2+x}U^{IV}_{2-x}An^{III}_{x}(C_2O_4)_5{\cdot}nH_2O$ (Tamain, Grandjean, Arab-Chapelet, & Abraham, 2010). This confirms the conclusions drawn from the FTIR analysis of experiment 3. Additional peaks present between 35-55 2Θ not present in the literature suggest an additional phase such as An(III) oxalate was also present in the structure indicating that the precipitate was not single phased.

Mixed oxalates typically fall within three different structure categories named, triclinic, hexagonal and tetragonal and are characterised by both metallic cations located on the same site leading to the formation of solid solutions. This partial occupation can occur as the ions of actinide (IV) and actinide (III)/lanthanide(III) can exhibit the same coordination sphere. Studies within the literature on single crystal XRD have enabled the identification of each of these three structure categories. Triclinic compounds have the formula, $M_{1-x}[An^{III}_{1-x}An^{IV}_{x}(C_2O_4)_2{\cdot}H_2O]{\cdot}nH_2O$ and can be described by the space group P-1. Each actinide ion is 9 coordinated surrounded by four oxalate ligands and 1 water molecule displaying tunnels with elliptic cross sections in 3-dimensions. The tetragonal structure has the same generic formula as the triclinic structure with a space group of P4/n. The 2-dimensional structure is also nine-fold coordinated with four bidentate oxalate ions and one water molecule. The polyhedral forming the structure can be described as mono-capped square antiprisms. The hexagonal structure, space group $P6_3/mmc$, has the generic formula $M_{2+x}U^{IV}_{2-x}An^{III}_{x}(C_2O_4)_5{\cdot}nH_2O$. Hexagonal compounds comprise a 3-dimensional honeycomb like structure where the metallic cations are ten-fold coordinated from 5 bis-bidentate oxalate groups (Tamain, Grandjean, Arab-Chapelet, & Abraham, 2010).

From the combined FTIR and XRD data, this suggests that experiments 1 and 2 had formed a tetragonal structure with the formula, $M_{1-x}[An^{III}_{1-x}An^{IV}_{x}(C_2O_4)_2{\cdot}H_2O]{\cdot}nH_2O$ and experiment 3 had formed mainly a hexagonal structure with the generic formula, $M_{2+x}An^{V}_{2-x}An^{III}_{x}(C_2O_4)_5{\cdot}nH_2O$; where M is the counter cation, in this case likely a hydrazinium cation ($N_2H_5^+$).

This project has received funding from the EURATOM research and training programme 2014-2018 under grant agreement No 755171. The content of this deliverable reflects only the author's view. The European Commission is not responsible for any use that may be made of the information it contains.

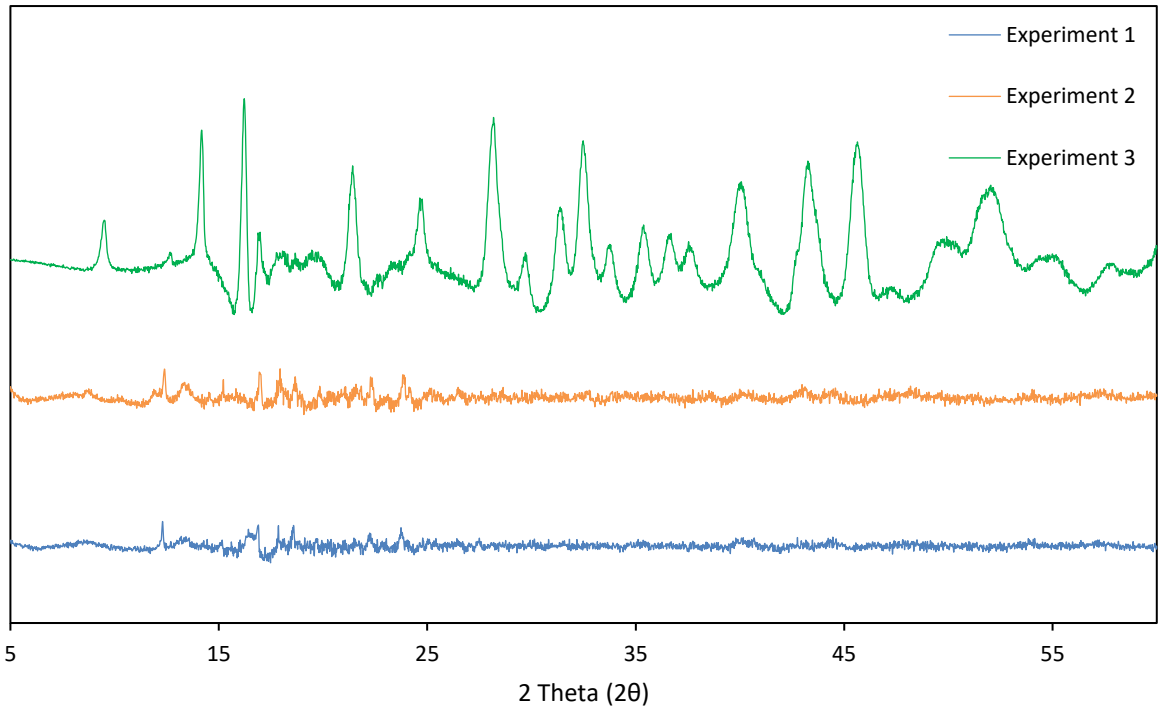

Figure 20: X-ray diffraction pattern of each mixed oxalate produced prior to calcination.

OXALATE DECOMPOSITION AND CALCINATION

Each mixed oxalate was decomposed on a hotplate prior to co-calcination at the desired temperature due to the potential deflagration risk during decomposition of mixed oxalates. As this was an intermediate conversion stage, no analyses were completed on the mixed oxides after decomposition on the hotplate. A summary of the mass losses following decomposition and calcination are presented in Table 6, Table 7 and Table 8. The measured mass losses were lower than expected according to the theoretical mass loss indicating the potential absorption of organics during decomposition. Further information will be given once the carbon analysis data becomes available.

This project has received funding from the EURATOM research and training programme 2014-2018 under grant agreement No 755171. The content of this deliverable reflects only the author's view. The European Commission is not responsible for any use that may be made of the information it contains.

Table 6: Mass losses during decomposition on a hotplate.

Experiment	Mass before decomposition / g	Mass after decomposition / g	Measured mass loss / g	Theoretical mass loss / g	Measured mass loss / wt%
Experiment 1	7.80	4.99	2.81	3.92	36
Experiment 2	8.67	4.99	3.68	4.36	42
Experiment 3	6.03	3.52	2.51	2.90	42

Table 7: Summary of mass losses after calcination of mixed (U,Pu, Np) oxides under an air atmosphere.

Experiment/Conditions	Mass before calcination / g	Mass after calcination / g	Mass loss / g	Mass loss / wt%
Experiment 1/ 650 °C Air	2.46	2.38	0.08	3
Experiment 1/ 900 °C Air	2.51	2.43	0.08	3
Experiment 2 / 650 °C Air	2.49	2.44	0.05	2
Experiment 2 /900 °C Air	2.49	2.43	0.06	2

Table 8: Summary of mass losses after calcination of mixed (U, Pu, Np) oxides under an argon atmosphere.

Experiment/Conditions	Mass before calcination / g	Mass after calcination / g	Mass loss / g	Mass loss / wt%
Experiment 3 / 650 °C Argon	1.75	1.67	0.08	5
Experiment 3 / 900 °C Argon	1.77	1.68	0.09	5

This project has received funding from the EURATOM research and training programme 2014-2018 under grant agreement No 755171. The content of this deliverable reflects only the author's view. The European Commission is not responsible for any use that may be made of the information it contains.

INFRARED ANALYSIS

Infrared analysis was completed on each of the six oxides produced and the overlaying spectra are presented in Figure 21 and the approximate absorption bands in Table 9. Each oxide was analysed in triplicate with excellent agreement between the results noting only a single spectrum from each set is presented in Figure 21. Broad absorption bands between 3000-4000 cm^{-1} are attributed to the overlap of various water coordination and vibration modes from water molecules present in the structure. Each oxide also has weak band centred at 2930 cm^{-1} indicating a strongly bonded H-O-H stretch (Webb, et al., 2019). Another common broad absorption band at 1750 cm^{-1} has been reported in the literature as a C=O stretch and is commonly seen in the decomposition of Nd and Ce oxalates (Almeida, Grandjean, Vigier, & Patisson, 2012) (Gabal, Elroby, & Obaid, 2012). Medium/weak absorption bands at 2700 and 2645 cm^{-1} are only present in spectra from experiments 1 and 2 with no obvious assignments for these bands found in the literature. Another weak absorption band present in experiments 1 and 2 centred at 2325 cm^{-1} has also been observed in some recent (U,Pu) oxalate decomposition experiments suggesting that it is due to atmospheric CO_2 in the product likely from the decomposition of the oxalate. Experiment 2 which apparently included PTD and acetic acid within the oxalate shows no signs of these species left in the oxide product suggesting that if PTD was not destroyed during evaporation stages it would have no overall effect on the oxide product.

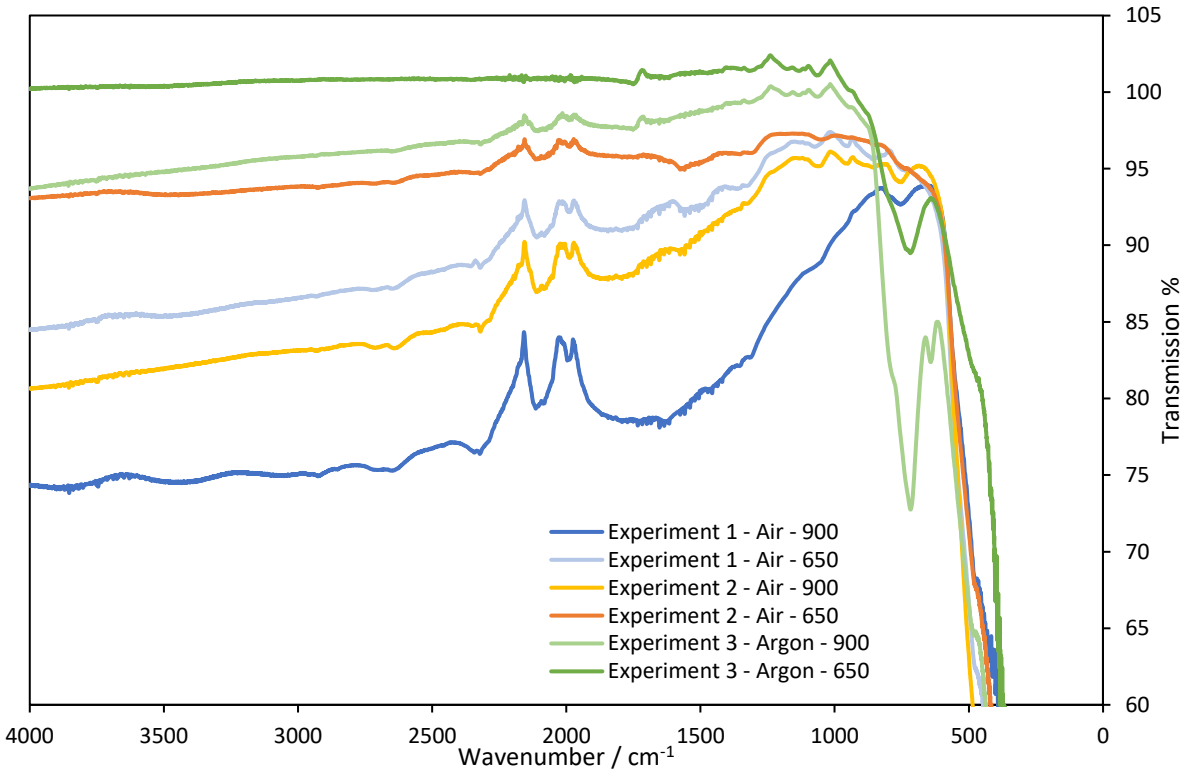

Figure 21: Infrared spectra of GANEX TRU oxides following calcination at 650 °C and 900 °C in either an air or argon atmosphere.

This project has received funding from the EURATOM research and training programme 2014-2018 under grant agreement No 755171. The content of this deliverable reflects only the author's view. The European Commission is not responsible for any use that may be made of the information it contains.

Table 9: Infrared absorption bands for each oxide decomposition product.

Wavenumber/ cm^{-1}	Experiment 1		Experiment 2		Experiment 3		Tentative assignments
	900 °C air	650 °C air	900 °C air	650 °C air	900 °C argon	650 °C argon	
3800	s, br	Br					H_2O - overlap of various water coordination and vibration modes
3400	s, br	s, br	vw, br	m, br	vw, br	vw, br	H_2O - overlap of various water coordination and vibration modes
3000	s, br						H_2O - overlap of various water coordination and vibration modes
2930	m/w	w	w	w	w	vw	strong H-bonded H-O-H stretch
2850	w		w				
2700	m/w	m/w	m	m/w			Ln oxalate decomposition product
2645	m/w	m/w	m	m/w	w		
2325	w	w	vw	w	vw		CO_2 - from decomposition of oxalate
1750	m, br	m, br	s, br	w, br	m, br	m	a C=O stretch
1620	w				w, br	m	H_2O, bending δ(H-O-H)
1550			sh, br	s, br			possibly carbonate, or 2LO1+LO2 transition
1500	m, br	m, br					possibly carbonate
1350	w	m/w, br	w	w	w	m	possibly carbonate
1310	w	w		w	w	m	Possibly bicarbonate
1250			sh				probably an adsorbed species (C-N or C-O based stretch)
1180					w	m	Possibly 2LO2
1130					w	m	Possibly 2LO2
1060	sh	m	m	m	w	m	ωLO + ωR
970	sh		m				
950		m				sh	possibly 2TO2 or Γ_1-Γ_4, maybe neither
930	sh			w	w		possibly 2TO2 or Γ_1-Γ_4,
850		m	m,br	w			possibly carbonate
750	s/m	w	s/m	sh	vs	s	probably 2 x ω0P
640					m		Possibly ωLOx in UO_2

Note: s-strong; m-medium; w-weak; vw--very weak; br--broad; v br--very broad; vvw --very weak; sh-shoulder

This project has received funding from the EURATOM research and training programme 2014-2018 under grant agreement No 755171. The content of this deliverable reflects only the author's view. The European Commission is not responsible for any use that may be made of the information it contains.

X-RAY DIFFRACTION ANALYSIS

Due to time constraints imposed by COVID-19 there was only sufficient time to prepare and analyse the oxide samples calcined at 650 °C and therefore the 900 °C oxides will be reported in a future issue of this report. The XRD patterns for each oxide decomposed at 650 °C are presented in Figure 22. Comparing experiments 1 and 2, these were oxides produced under identical conditions apart from the addition of PTD and acetic acid during oxalate precipitation of experiment 2; both oxalates were decomposed and calcined in an air atmosphere. The diffraction patterns are almost identical with a slight shift in 2Θ for the oxide containing PTD/acetic acid. The peaks are broad and are characteristic of defects in the crystal lattice caused by alpha decay. This generates Frenkel pair defects as oxygen and metal atoms are displaced from their lattice positions, creating interstitial atoms and vacancies that have the potential to cause an increase in the lattice volume. Defects are generated by collisions of both the alpha particles and the recoil uranium atom, the latter contributing to a large fraction of the defects (Orr & Colledge, 2018). Comparison of the diffraction patterns for experiments 1 and 2 with literature data shows the reflections are characteristic of a pure single phase oxide MO_2 with a space group of Fm-3m. Figure 23 shows the diffraction patterns from experiment 1 and 2 with the diffraction pattern of a recent production Magnox PuO_2 sample overlayed. The Magnox PuO_2 sample was calcined at 600 °C under air and is virtually identical to the oxides produced here. These results suggest that the addition of additional An(III) metal ions and complexants (PTD) and their potential degradation products (acetic acid) would have no effect on the final structure of the oxide product.

Experiment 3 was a mixed oxide consisting of U(IV) – An(III) (where An(III) = Pu, Nd and Sm) that was decomposed under air but calcined in argon. The diffraction pattern has some of the key peaks associated with an MO_2 phase however, there are additional peaks that were not present in experiments 1 and 2, and suggest the formation of a $(U, M)_3O_8$ phase. Pawley whole pattern fitting using TOPAS-5 with an Fm-3m and C2mm space group for a $(U,Pu)O_2$ and $(U, An(III))_3O_8$ hkl phase respectively produced an excellent fit. The presence of >50 % U(IV) within a mixed oxalate structure was always a concern as to whether a single phase mixed oxide could be produced. Unfortunately due to lab challenges it was not possible to decompose experiment 3 under an argon atmosphere and therefore the formation of the M_3O_8 phase was likely during decomposition as pure MO_2 probably requires a reducing atmosphere during calcination. The formation of oxides with an oxygen to metal ratio greater than 2 has been reported for UO_2- rich compounds that have been heat treated in air (Elorrieta, et al., 2017). The formation of U_3O_8 is problematic for nuclear fuel production as this involves an increase in volume of ~36% that has the potential to affect the integrity of the fuel and therefore safety challenges during storage (Elorrieta, et al., 2017).

Pawley fitting allowed a preliminary determination of the lattice parameter(s) and crystallite size for each oxide and the results are presented in Table 10. The lattice parameters can be compared to Vegards-law where a plot of the lattice parameters at x = 0 (i.e. 5.433 Å for NpO_2 or 5.471 Å for UO_2) and x = 100 (i.e. 5.396 Å for PuO_2) are connected by a straight line as shown in Figure 24 (for exp 1 and 2) and Figure 25 (for exp 3) (Leinders, Cardinaels, Binnemans, & Verwerft, 2015) (Nandi, Danny, Bhattacharya, Prakash, & Behere, 2021) (Yamashita, Nitani, Tsuji, & Inagaki, 1997). The variation of lattice parameter with composition is found to follow Vegard's law for experiments 1 and 2 however, experiment 3 deviates due to the formation of an $(U,M)_3O_8$ phase.

This project has received funding from the EURATOM research and training programme 2014-2018 under grant agreement No 755171. The content of this deliverable reflects only the author's view. The European Commission is not responsible for any use that may be made of the information it contains.

Table 10: Lattice parameter(s) and crystallite size for each oxide produced determined using Pawley whole pattern fitting.

		Lattice parameter(s) / Å		Crystallite size / nm
Experiment 1		a	5.39980 ± 0.00003	10.11
Experiment 2		a	5.39955 ± 0.00003	10.79
Experiment 3	$(U,M)O_{2+x}$ ***(Fm-3m)***	a	5.41214 ± 0.00030	8.36
	$(U,M)_3O_8$ ***(C2mm)***	a b c	6.74450 ± 0.00147 11.8267 ± 0.00123 4.14914 ± 0.00042	-

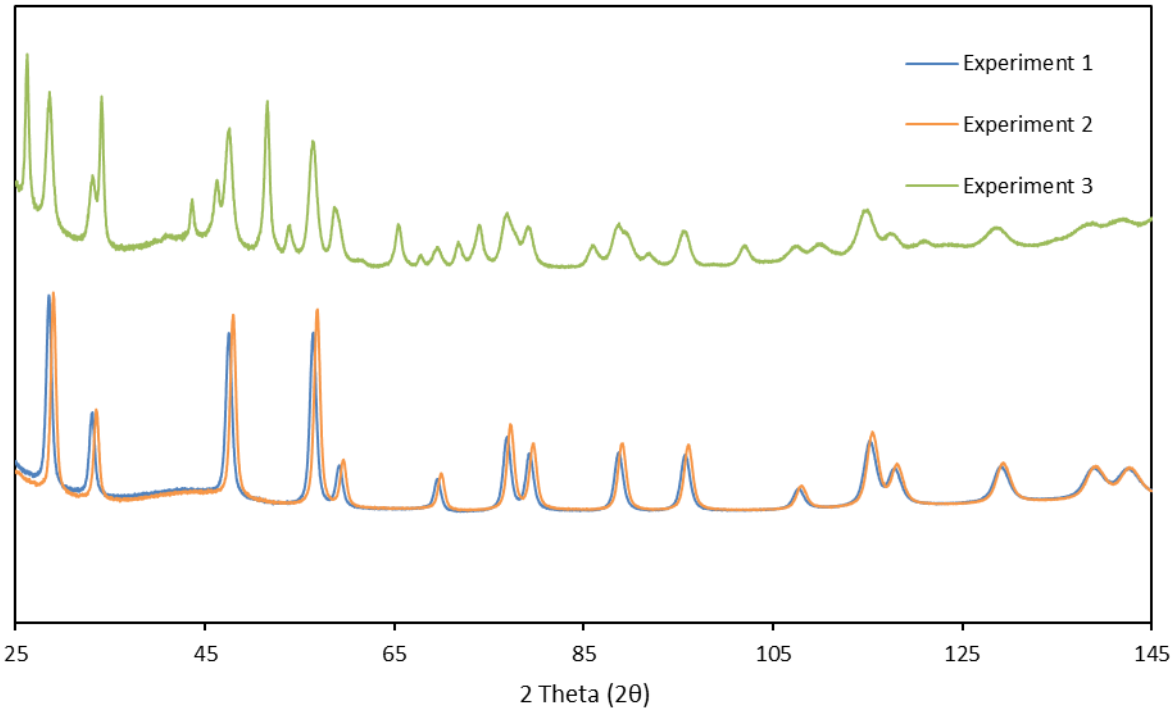

Figure 22: X-Ray Diffraction patterns for each mixed oxide produced.

This project has received funding from the EURATOM research and training programme 2014-2018 under grant agreement No 755171. The content of this deliverable reflects only the author's view. The European Commission is not responsible for any use that may be made of the information it contains.

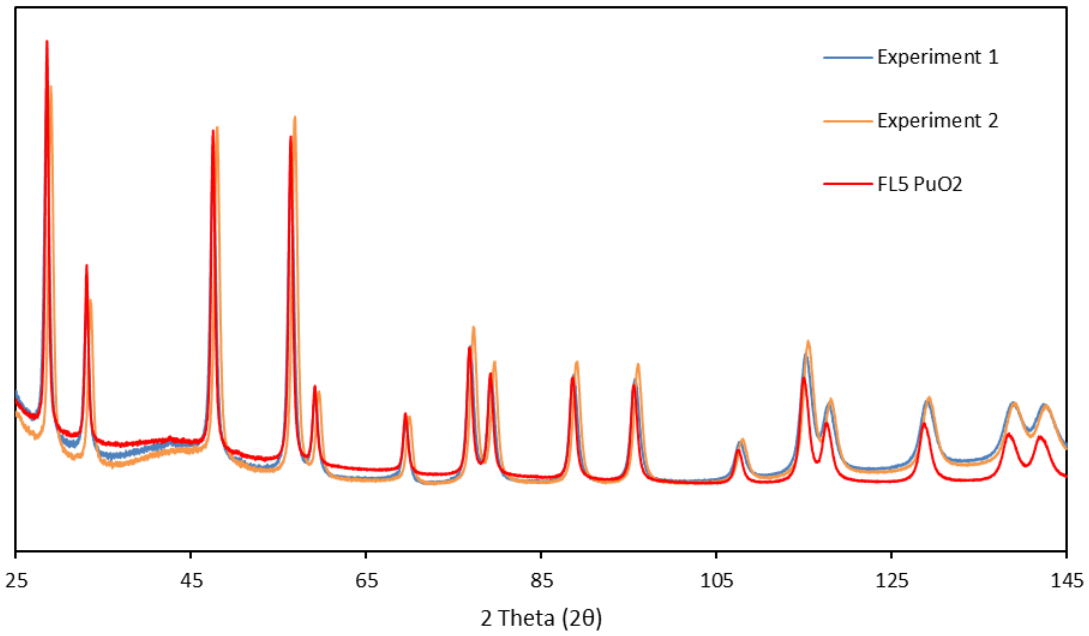

Figure 23: XRD pattern for experiments 1 and 2 with a recent production PuO_2 oxide overlayed (in red).

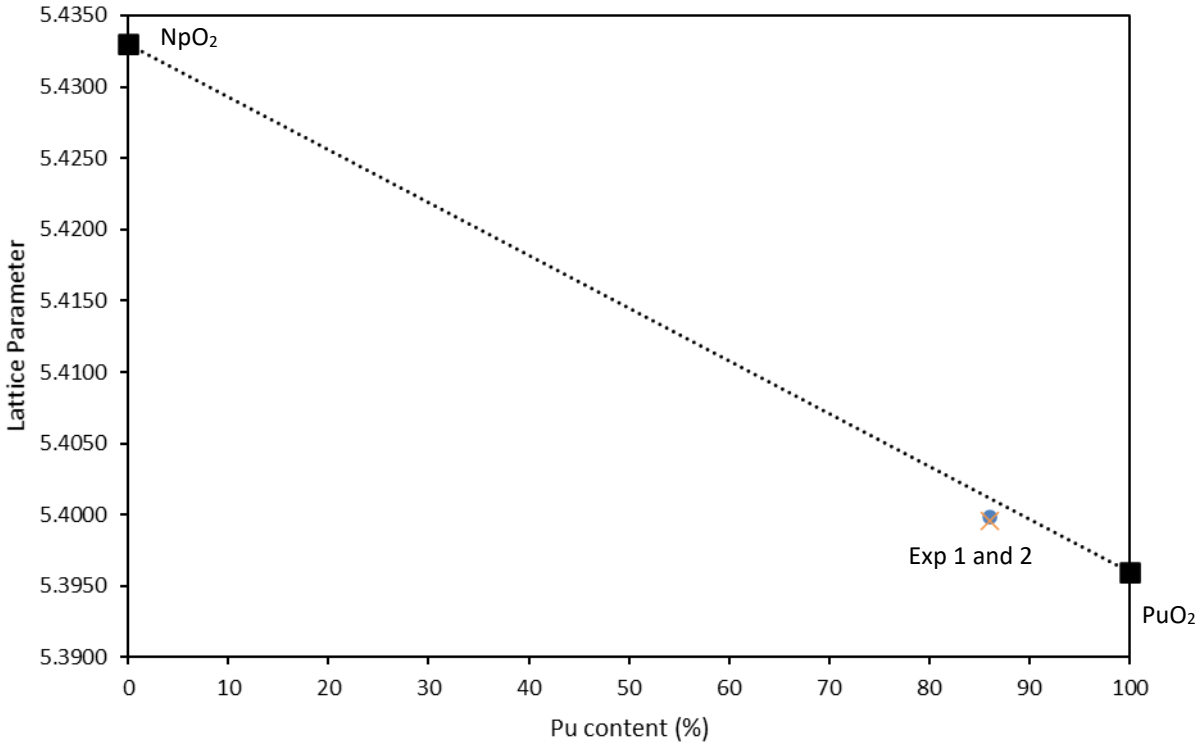

Figure 24: Lattice parameters as a function of Pu content. The dashed line represents values predicted by Vegards law, taking as reference NpO_2 and PuO_2 experimental lattice parameters.

This project has received funding from the EURATOM research and training programme 2014-2018 under grant agreement No 755171. The content of this deliverable reflects only the author's view. The European Commission is not responsible for any use that may be made of the information it contains.

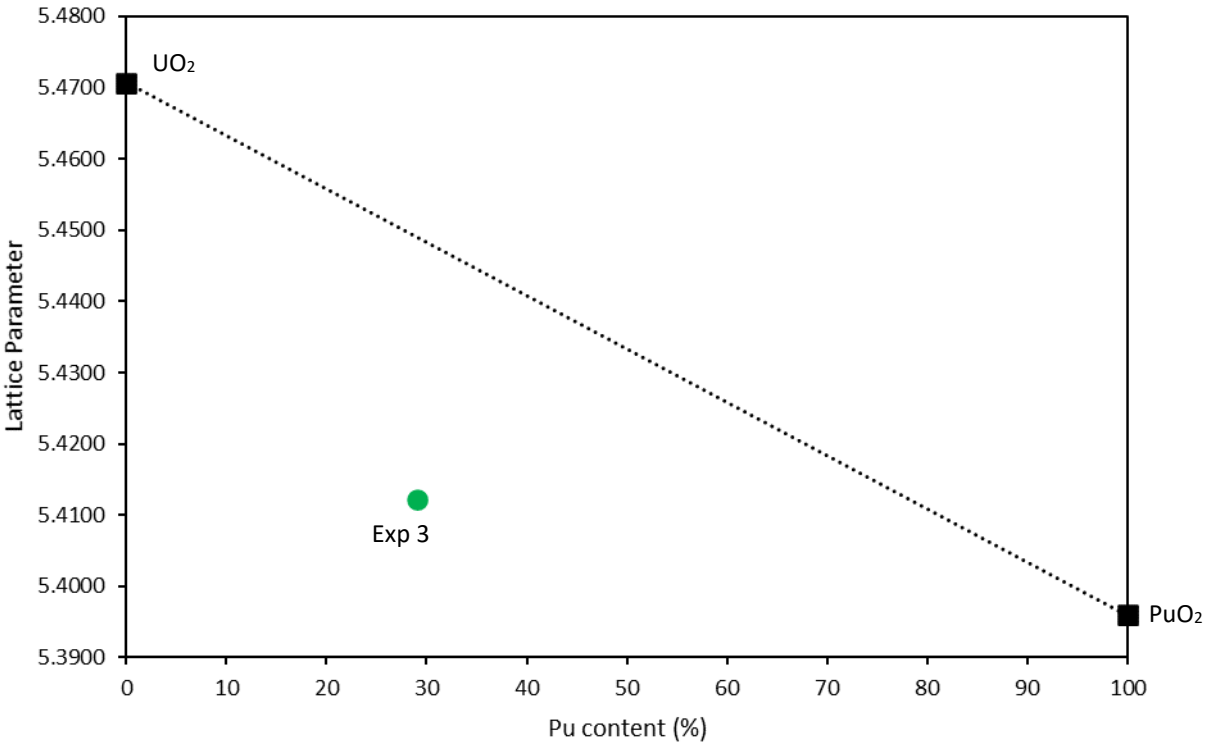

Figure 25: Lattice parameters as a function of Pu content. The dashed line represents values predicted by Vegards law, taking as reference UO_2 and PuO_2 experimental lattice parameters .

SPECIFIC SURFACE AREA ANALYSIS

The specific surface area of the product oxide is controlled by the calcination temperature and atmosphere during decomposition of the oxalate with limited data to show that the time at temperature has any effect on the measured SSA. Literature studies have suggested that the surface area initially increases between 200-400 °C due to fracturing of particles as water and gases escape and then as the temperature increases above 400 °C the specific surface area begins to decrease due to growth of the crystallites (Orr, Simms, & Taylor, 2015). Oxides produced via the oxalate route are expected to have a surprisingly high SSA that is believed to be due to the particle size and high internal porosity. The literature also suggests that the atmosphere used during calcination can also influence the measured SSA of Pu(IV) oxide with higher SSA recorded under an argon atmosphere compared to air but at the same temperature (Vigier, Grandjean, Arab-Chapelet, & Abraham, 2007).

Specific surface area analysis was completed on each of the oxides following decomposition and the results are presented in Table 11. As the calcination temperature increased from 650 to 900 °C the SSA decreases considerably regardless of the initial feed mixture and is in agreement with the literature and subsequent growth of the crystallites (Machuron-Mandard & Madic, 1996). The variation in SSA at 650 °C for experiments 1 and 2 is unknown but is likely to be within the range expected of an oxide produced via oxalate precipitation. The target SSA for nuclear fuel, according to reference (Collins, Voit, & Vedder, 2011), is between 2-30 m^2/g with traditional MOX prepared via UO_2 and PuO_2 with SSA at 4 and 10 m^2/g respectively. Further, the SSA of experiment 3 calcined at 650 °C is considerably lower than the SSA of experiments 1 and 2 calcined at the same temperature but differing atmospheres; this contradicts the paper by Vigier et al (2007) although these

This project has received funding from the EURATOM research and training programme 2014-2018 under grant agreement No 755171. The content of this deliverable reflects only the author's view. The European Commission is not responsible for any use that may be made of the information it contains.

measurements were reported for Pu(IV). Literature studies suggest that batch size could have a significant effect on the measured SSA and could be the cause of the variation between the results presented here and the literature data. Additional studies would be required to confirm this. The values measured are within this approximate range; however, it is important to note that the final sintered density and microstructure of the resultant fuel pellet will be a function of various powder properties including powder morphology and flowability and not just SSA. Unfortunately, it was not possible to evaluate the morphology of the resultant oxides.

Table 11: Specific surface area of each oxide product.

	Experiment 1		Experiment 2		Experiment 3	
Calcination conditions	**900 °C air**	**650 °C air**	**900 °C air**	**650 °C air**	**900 °C argon**	**650 °C argon**
SSA (m^2/g)	5.01	24.36	3.70	16.79	2.78	8.74

CARBON ANALYSIS

Each GANEX TRU oxide was sent to Sellafield's Analytical Services (SLAS) for carbon analysis to determine the extent of carbon contamination in each oxide product. Unfortunately, the SLAS coulomat instrument used to analyse the samples is out of service and therefore the results will be reported in a future issue of this report once data becomes available. For fuel manufacture, the level of carbon contamination is typically expected to be <100 ppm and is one of the major disadvantages of the oxalate route as calcination temperature and atmosphere can have a detrimental effect on the carbon content of the oxide (Orr, Simms, & Taylor, 2015). Residual carbon is usually caused by the either the disproportionation of CO during decomposition (Eq 1) or incomplete decomposition of the oxalate. However, alternative surface reactions, such as Eq 2, have also been suggested. Within an air atmosphere any CO produced should be oxidised to CO_2 (Eq 3) particularly in the presence of water this reaction is accelerated (Eq 4) suggesting that calcinations at higher temperatures under air will lead to the least residual carbon in the oxide product (Orr, Simms, & Taylor, 2015). However, within an air atmosphere there is the potential for U(IV) to be reoxidised to U(VI) that could create inhomogeneity in the resultant oxide and the formation of separated U_3O_8 and PuO_2 phases. This is a potential drawback to decomposition and calcination under air and therefore alternative atmospheres and temperatures have been considered here to determine their effects on the quality of the product oxide. Further details and results will be reported once data become available.

$$2CO \rightarrow C + CO_2 \qquad \text{Eq 1}$$

$$PuO_{(2-x)} + xCO \rightarrow PuO_2 + xC \qquad \text{Eq 2}$$

$$2CO + O_2 \rightarrow CO_2 \qquad \text{Eq 3}$$

$$CO + H_2O \leftrightarrow CO_2 + H_2 \qquad \text{Eq 4}$$

This project has received funding from the EURATOM research and training programme 2014-2018 under grant agreement No 755171. The content of this deliverable reflects only the author's view. The European Commission is not responsible for any use that may be made of the information it contains.

CONCLUSIONS

A study related to the product finishing has been carried out covering the preparation of EURO-GANEX transuranic mixed oxides and characterisation of their suitability for re-use as nuclear fuel. Unfortunately, due to challenges imposed by COVID-19, some analyses are outstanding therefore making comprehensive conclusions difficult to make at this time. A further update will be provided once a complete data set is available.

From the evidence available to date, a mixed TRU feed was successfully prepared by electrochemical conditioning of Pu(IV)/Np(V) and U(VI) with the addition of Nd(III) and Sm(III) as An(III) surrogates. This method worked well in the presence of a hydrazine stabiliser. However, due to the challenges in replicating this within an industrial environment, work is ongoing to consider alternative methods of reduction. Oxalate co-precipitation was successful with an excellent recovery of metal nitrates to the solid mixed oxalate. Further, the presence of PTD and acetic acid in the feed mixture had no noticeable effect on the either the solubility of the metal nitrates in solution or the resultant structure of the oxalate /oxide product. Infrared analysis of the oxalates confirmed the formation of a hexagonal structure for experiment 1 and 2 (TRU oxalate) and a tetragonal structure for experiment 3 (U(IV): TRU oxalate) and is in good agreement with literature studies. Analysis of the oxalates by XRD was challenging due to the low crystallinity of the material but appeared to confirm conclusions drawn by FTIR analysis. (Note that this work was not intended to optimise the conditions of the oxalate precipitation step and there remains the opportunity to adjust the processing parameters such as temperature or mixing rates to do this).

Following decomposition and calcination, analysis of the oxide products revealed that the TRU oxides produced a cubic MO_2 structure that was comparable to PuO_2 produced on the Magnox finishing lines both in terms of structure and specific surface area. The U(IV):TRU oxide formed a mixed phase product containing MO_2 and $(U,M)_3O_8$ phases and re-oxidation of the U(IV) was likely caused during decomposition under air prior to calcination under argon. Unfortunately, the levels of carbon contamination in each of the oxides was not available at the time of writing this report.

This study provides a good basis for the finishing of a GANEX TRU product and proves the initial concept of precipitation and calcination of a mixed transuranic nitrate product from a chemical separation flowsheet. Further, the negligible effect of the addition of the complexant, PTD, and potential degradation products, on the quality of the oxide product is promising. Going forward, further process optimisation on the calcination of a mixed U(IV)-TRU oxalate is required and how to maintain a solid solution during decomposition whilst minimising the levels of carbon contamination that may be detrimental to the quality of the oxide. An alternative method of calcination by decomposing in air to reduce the levels of carbon contamination followed by calcination under a reducing atmosphere could be considered to re-reduce any U_3O_8 formed back to UO_2. In addition, it would be important to consider effects of oxalate precipitation on the morphology of the oxide by investigating changes in temperature, mixing regime of oxalic acid and digestion time and whether this would have an effect on the quality of the oxide produced. This would then require optimisation of the pelleting process to determine the sintering conditions that would be required to produce nuclear fuel that has the potential to be reused in a Gen(IV) reactor.

Following this study, the following recommendations should be considered for a future phase of work:

- investigate the effects of a reducing atmosphere during calcination of a mixed (U,TRU) oxalate to determine whether a solid solution oxide can be maintained with minimal levels of carbon contamination,
- complete a series of small scale studies testing the effects of temperature, mixing regime and digestion time on the morphology of the resultant oxalate,

This project has received funding from the EURATOM research and training programme 2014-2018 under grant agreement No 755171. The content of this deliverable reflects only the author's view. The European Commission is not responsible for any use that may be made of the information it contains.

- once processing conditions have been optimised complete a series of sintering trials to determine the quality of the final TRU oxide fuel pellet.

This project has received funding from the EURATOM research and training programme 2014-2018 under grant agreement No 755171. The content of this deliverable reflects only the author's view. The European Commission is not responsible for any use that may be made of the information it contains.

REFERENCES

Almeida, L. D., Grandjean, S., Vigier, N., & Patisson, F. (2012). Insights into the Thermal Decomposition of Lanthanide(III) and Actinide(III) Oxalates – from Neodymium and Cerium to Plutonium. *Eur. J. Inorg. Chem*, 4986–4999.

Ansari, A., Pathak, P., Manchanda, V., Husain, M., Prasad, A., & Parmar, V. (2005). N, N, N, N-Tetraoctyl diglycolamide (TODGA): A promising extractant for Actinide-partioning from high-level waste (HLW). *Solvent Extraction Ion Exhange*, 463-479.

Arab-Chapelet, B., Grandjean, S., Nowogrocki, G., & Abraham, F. (2007). Synthesis of new mixed actinides oxalates as precursors of actinides oxide solid solutions. *Journal of Alloys and Compounds* , 387–390.

Arab-Chapelet, B., Grandjean, S., Nowogrocki, G., & Abraham, F. (2008). Synthesis and characterization of mixed An(IV)An(III) oxalates (An(IV) = Th, Np, U or Pu and An(III) = Pu or Am). *Journal of Nuclear Materials*, 259–268.

Bell, K., Carpentier, C., Carrot, M., Geist, A., Gregson, C., Heres, X., . . . Wilden, A. (2012). Progress towards the development of a new GANEX process. *Procedia Chemistry*, 392-397.

Birkett, J., Carrott, M., Fox, O., Jones, C., Maher, C., Roube, C., . . . Woodhead, D. (2005). Recent development in the PUREX process for Nuclear fuel reprocessing complexant based stripping for uranium and plutonium separation. *Chimia*, 898-904.

Brown, J., Carrott, M., Fox, O., Maher, C., Mason, C., McLachlan, F., . . . Woodhead, D. (2010). IOP Coference Series: Materials Science and Engineering.

Brown, J., McLachlan, F., Sarsfield, M., Taylor, R., Modolo, G., & Wilden, A. (2012). Plutonium loading of prospective grouped actinide extraction (GANEX) solvent based systems based on diglycolamide extractants. *Solvent Extraction and Ion Exchange*, 127-141.

Campbell, C., Gregson, C., Orr, R., Sims, H., Taylor, R., & Webb, K. (2014). *Results of heat treatment experiments on chloride contaminated PuO2 samples* . NNL (14) 12869.

Carrott, M., Bell, K., Brown, J., Geist, A., Gregson, C., Heres, X., . . . Taylor, R. (2014). Development of a New Flowsheet for Co-Separating the Transuranic Actinides: The "EURO-GANEX" Process. *Solvent Extraction and Ion Exchange*, 447-467.

Carrott, M., Geist, A., Heres, X., Lange, S., Malmbeck, R., Miguirditchian, M., . . . Taylor, R. (2015). Distribution of plutonium, americium and interfering fission products between nitric acid and mixed organic phase of TODGA abd DMDOHEMA in kerosene, and implications for the design of the "EURO-GANEX" process. *Hydrometallurgy, no 152*, 139-148.

Collins, E., Voit, S., & Vedder, R. (2011). *Evaluation of Co-precipitation Processes for the Synthesis of Mixed-Oxide Fuel Feedstock Materials.* ORNL, United States.

Dhamodharan, K., & Pius, A. (2016). Determination of Plutonium Present in Highly Radioactive Irradiated Fuel Solution by Spectrophotometric Method. *Nuclear Engineering and Technology*, 727-732.

This project has received funding from the EURATOM research and training programme 2014-2018 under grant agreement No 755171. The content of this deliverable reflects only the author's view. The European Commission is not responsible for any use that may be made of the information it contains.

Elorrieta, J. M., Manara, D., Bonales, L. J., Vigier, J. F., Dieste, O., Naji, M., . . . Cobos, J. (2017). Raman study of the oxidation in (U,Pu)O2 as a funcation of Pu content. *Journal of Nuclear Materials*, 484-491.

(2020). *FRFR2: gPROMS model of GANEX process developed.* BEIS10993/06/26/06 - ISSUE 1.

Gabal, M., Elroby, S. A., & Obaid, A. (2012). Synthesis and characterization of nano-sized ceria powder via oxalate decomposition route. *Powder Technology*, 112–118.

Govindarajan, S., Patil, K. C., Poojary, M. D., & Manohar, H. (1986). Synthesis, Characterization and X-ray Structure of Hexahydrazinium Diuranyl Pentaoxalate Dihydrate, (N,H,)6(U02)2(Cz04) 5l2H20. *Inorganica Chimica Acta*, 103-107.

Jaffe, D. A., & Rose, N. (1991). The heat of dimerization of acetic acid and the heat of decomposition of ammonium acetate as determined by FTIR spectroscopy. *Spectrochimica Acta*, 1695-1705.

Joly, P., & Boo, E. (2015). *Roadmap: Actinide separation processes 2015.* SACSESS.

Krishnakumar, V., Jayamani, N., & Mathammal, R. (2011). Molecular structure, vibrational spectral studies of pyrazole and 3,5-dimethyl pyrazole based on density functional calculations. *Spectrochimica Acta Part A*, 1959–1968.

Leinders, G., Cardinaels, T., Binnemans, K., & Verwerft, M. (2015). Accurate lattice parameter measurements of stoichiometric uranium dioxide. *Journal of Nuclear Materials*, 135-142.

Macerata, E., Mossini, S., Scaravaggi, S., Mariani, M., Mele, A., Panzeri, W., . . . Casnati, A. (2016). Hydrophilic clicked 2,6-Bis-triazoyl-pyridines endowed with high actinide selectivity and radiochemical stability: Toward a closed nuclear fuel cycle. *J. Am. Chem Soc*, 7232-7235.

Machuron-Mandard, X., & Madic, C. (1996). Plutonium dioxide particle properties as a function of calcination temperature. *Journal of Alloys and Compounds*, 216–224.

Malmbeck, R., Carrott, M., Geist, A., Heres, X., Miguirditchian, M., Modolo, G., . . . Wilden, A. (2014). The hydrometallurgical co-separation of Neptunium, Plutonium, Americium and Curium by the Euro-GANEX Process. *20th International Solvent Extraction Conference, 7-11 September 2014.*

Malmbeck, R., Magnusson, D., Bourg, S., Carrott, M., Geist, A., Hérès, X., . . . Wilden, A. (2019). Homogenous recycling of transuranium elements from irradiated fast reactor fuel by the EURO-GANEX solvent extraction process. *Radiochimica Acta*, 917-929.

Miguirditchian, M., Chareyre, L., Sorel, C., Bisel, P., Baron, P., & Masson, M. (2008). Development of the GANEX process for the reprocessing of GEN IV spent nucelar fuels. *Atlante 2008*, 1-4.

Modolo, G., Asp, H., Schrienemachers, C., & Vijgen, H. (2012). Development of a TODGA based process for the partioning of actinides from a PUREX raffinate. Part I: Batch extraction optimisation studies and stability tests. *Solvent extraction and Ion Exhange*, 127-141.

Modolo, G., Wilden, A., Kaufholz, P., Bosbach, D., & Geist, A. (2014). Development and demonstration of innovative partitioning processes (i-SANEX and 1-cycle SANEX) for actinide partitioning. *Progress in Nuclear Energy*, 107-114.

This project has received funding from the EURATOM research and training programme 2014-2018 under grant agreement No 755171. The content of this deliverable reflects only the author's view. The European Commission is not responsible for any use that may be made of the information it contains.

Mossini, E., Macerata, E., Brambilla, L., Panzeri, W., Mele, A., Castiglioni, C., & Mariani, M. (2019). Radiolytic degradation of hydrophilic PyTri ligands for minor actinide recycling. *Journal of Radioanalytical and Nuclear Chemistry*, 1663-1673.

Nandi, C., Danny, K., Bhattacharya, S., Prakash, A., & Behere, P. (2021). Phase evolution in M1-xPuxO2 (0.0 ≤ x ≤ 0.6) (M = Zr, Th) as potential inert matrix fuel system under reducing and oxidizing conditions. *Journal of Nuclear Materials*, 152800.

Orr, R., Simms, H., & Taylor, R. (2015). A review of plutonium oxalate decomposition reactions and effects of decomposition temperature on the surface area of the plutonium dioxide product. *Journal of Nuclear Materials* , 756-773.

Poinsott, C., Rostaing, C., Baron, P., Warin, D., & Boullis, B. (2012). Main results of the French program on partioning of minor actinides, a significant improvement towards nucelar waste reduction. *Procedia Chem*, 358-366.

Rizkalla, E. N., & Choppin, G. R. (1992). Hydration of lanthanides and actinides in solution. *Journal of Alloys and Compounds*, 325-336.

Tamain, C., Grandjean, S., Arab-Chapelet, B., & Abraham, F. (2010). Synthesis and structural characterisation of mixed An(IV)-An(III) actinide oxalates used as precurosrs for dedicated fuel or targets. *Proceedings of the First ACSEPT International Workshop.* Lisbon, Portugal.

Taylor, R., Carrott, M., Galan, H., Geist, A., Heres, X., Maher, C., . . . Wilden, A. (2016). The EURO-GANEX process: current status of flowsheet development and process safety studies. *Procedia Chemistry*, 524-529.

Vigier, N., Grandjean, S., Arab-Chapelet, B., & Abraham, F. (2007). Reaction mechanisms of the thermal conversion of Pu(IV) oxalate into plutonium oxide. *Journal of Alloys and Compounds*, 594–597.

Wagner, C., Mossini, E., Macerata, E., Mariani, M., Arduni, A., Casnati, A., . . . Panak, P. (2017). Time-Resolved Laser Fluorescence Spectroscopy Study of the Coordination Chemistry of the Hydrophilic CHON 1,2,3-Triazol-4-yl pyridine Ligand with Cm (III) and Eu(III). *Inorganic Chemistry*, 2135-2144.

Webb, K., Taylor, R., Campbell, C., Carrott, M., Gregson, C., Hobbs, J., . . . Sutherland-Harper, S. (2019). Thermal processing of chloride contaminated plutonium dioxide. *ACS Omega* , 12524-12536 .

Wilden, A. (2015). Laboratory-Scale Counter-Current Centrifugal Contactor Demonstration of an Innovative-SANEX Process Using a Water Soluble BTP. *Solvent extraction and Ion exchange*, 91-108.

Yamashita, T., Nitani, N., Tsuji, T., & Inagaki, H. (1997). Thermal expansions of NpO2 and some other actinide dioxides. *Journal of Nuclear Materials*, 72-78.

Zhu, Z., Sasaki, H., Suzuki, H., & Kimura, T. (2004). Cumalitive study on solvent extraction of elements by N, N, N`, N`-tetraoctyl-3-oxapentanediamide (TODGA) from nitric acid into n-dodecane. *Analytica Chimica Acta*, 163-168.

This project has received funding from the EURATOM research and training programme 2014-2018 under grant agreement No 755171. The content of this deliverable reflects only the author's view. The European Commission is not responsible for any use that may be made of the information it contains.